R. & M. No. 3087
(18,487)
A.R.C. Technical Report

MINISTRY OF SUPPLY

AERONAUTICAL RESEARCH COUNCIL
REPORTS AND MEMORANDA

Pressure-Plotting Measurements on an 8 per cent Thick Aerofoil with Trailing-Edge Flap Blowing

By

J. WILLIAMS, M.Sc., Ph.D., and A. J. ALEXANDER, B.Sc.,
of the Aerodynamics Division, N.P.L.

LONDON: HER MAJESTY'S STATIONERY OFFICE
1958
PRICE 12*s.* 0*d.* NET

Pressure-Plotting Measurements on an 8 per cent Thick Aerofoil with Trailing-Edge Flap Blowing

By

J. WILLIAMS, M.Sc., Ph.D., and A. J. ALEXANDER, B.Sc.,

of the Aerodynamics Division, N.P.L.

Reports and Memoranda, No. 3087*

June, 1956

Summary.—Wind-tunnel experiments were carried out on an 8 per cent thick aerofoil between end plates, with blowing from a slot in the knee of a 25 per cent chord trailing-edge flap, to improve the lifting efficiency of the flap. Both the blowing-slot width and position were varied. The sectional lift and pitching moment were derived by chordwise integration of the surface static pressures measured at the mid-span station. Tuft observations as well as surface-pressure measurements were made to determine the extent of the turbulent separation region on the trailing-edge flap and of the laminar separation bubble on the aerofoil nose.

The blowing momentum required to prevent flow separation on the flap, at a given flap angle and zero wing incidence, proved much less than might have been expected from earlier two-dimensional experiments on thicker wings with blowing over the flap from the shroud. This reduction is probably associated with the low effective aspect ratio of the present quasi two-dimensional model as well as with improvements in blowing techniques. The separation bubble on the aerofoil nose began to expand markedly (with the flap deflected) when the incidence reached only a few degrees, and simultaneously the blowing momentum needed to prevent flow separation on the flap tended to increase.

1. *Introduction.*—It is now well established that the effectiveness of trailing-edge flaps for increasing lift at constant incidence (and also $C_{L\,\max}$) can be considerably improved by blowing over the upper surface of the flap[1]. The plane jet emerging at high velocity from a narrow slot adheres to the upper surface and, by entraining slowly moving air, can suppress the flow separation on the flap and eventually increase the effective chord of the flap. Renewed interest in this method of boundary-layer control followed from Attinello's proposal that, with gas-turbine aircraft, high-pressure air bled from the compressor should be ducted directly (without expansion) to a choked blowing slot[2]. This so-called ' supersonic blowing ' scheme requires smaller ducts than the subsonic blowing schemes previously investigated. For, since the blowing pressures are higher, the mass flows required become correspondingly smaller to provide the same blowing momentum and also the air density in the duct is greater; both these factors are conducive to smaller ducts or duct velocities.

As a preliminary to wind-tunnel tests on a thin 60-deg delta wing with trailing-edge flap blowing, experiments of a fundamental nature have been made on an 8 per cent thick aerofoil between end plates, with blowing from a slot in the knee† of a 25 per cent chord trailing-edge flap. The experiments were a natural consequence of earlier National Physical Laboratory tests on this aerofoil with area suction on the upper surface of the trailing-edge flap, and of the David-Taylor Model-Basin tests[3] on a wing with supersonic blowing over the trailing-edge flap from the shroud‡. The

* Published with the permission of the Director, National Physical Laboratory.

† The exposed curved upper surface of the flap nose.

‡ Blowing from the shroud signifies that the slot is located in the upper surface of the wing just ahead of the flap.

area-suction investigation demonstrated that, as regards the prevention of flow separation over the flap, boundary-layer control need not be applied much ahead of the minimum-pressure point (with attached flow), which occurs about half-way round the flap knee. Furthermore, exploratory bench tests with supersonic blowing indicated that a simple cylindrical pipe duct (forming the round nose of the flap) would provide a reasonably uniform spanwise distribution, without elaborate ducting design. For these reasons, the present wind-tunnel tests were made with blowing from a slot in the flap knee, rather than from a slot in the shroud as in earlier work[1, 3]. An additional advantage was that modifications to the main body of the aerofoil were unnecessary, so that the suction flap tests could be pursued without hindrance. In practice, there may likewise be structural advantages in leading the compressed air from the fuselage into the flap rather than into the main body of the wing.

In the present paper, the results of pressure-plotting measurements from the trailing-edge flap blowing tests are presented, together with the sectional lift and pitching moment obtained by chordwise integration of the surface static pressures. The general characteristics of the flow over the aerofoil and flap are also discussed, but the boundary-layer and wake traverse work will be reported separately.

2. *Experimental Method.*—2.1. *Model Configuration and Arrangement in Tunnel.*—The aerofoil has an 8 per cent thick RAE 104 section, chosen from current low-drag sections because it offers a straight trailing-edge for almost the last 25 per cent chord (*i.e.*, the flap extent) and an acceptable thickness in the vicinity of the flap nose. The aerofoil chord was limited to 3 ft by tunnel constraint considerations, and the span to 3 ft by the then existing pumping and manufacturing facilities. The model was mounted vertically in the centre of the N.P.L. 9 ft × 7ft, No. 1 Tunnel, between fixed horizontal end-plates (*see* Figs. 1 and 2). The aerofoil and its trailing-edge flap were attached to independent turntables, both rotating about the flap hinge-line. The end-plates extended two-thirds span above and below the aerofoil chord-line, and two-thirds chord upstream and downstream of the aerofoil leading-edge and trailing-edge. This end-plate size was the largest feasible from the standpoint of accessibility to the model, and was found to give satisfactory flow over the tunnel working-section*. The set-up is quasi two-dimensional in the sense that the model generates a reasonably constant lift loading across the span, but has an effective aspect ratio of about 3·3 corresponding to its geometric aspect ratio of unity and the ratio 3/4 of aerofoil span to end-plate height[5]†.

In the wind-tunnel tests, the chordwise pressure distribution over the aerofoil upper and lower surfaces was measured near the mid-span station at about 45 static pressure holes; these were most closely spaced on the aerofoil nose and the front of the trailing-edge flap as shown in Fig. 4. Extra static tubes were inserted in the surface of the blowing tube so that each increment of 15 deg in flap angle exposed a further static hole on the flap knee just above the hinge-line. All the static pressures were recorded on multi-tube liquid manometers, together with the main-stream total head measured by a datum tube located in the working-section ahead of the model‡. Following the usual practice, the tunnel wind speed was controlled by balancing the tunnel gauge against the pressure difference between two rings of wall statics located at the beginning and the end of the tunnel contraction. The variation of main-stream velocity in the region between the end-plates with the model absent was found by pitot-static explorations to be less than $\pm$ 1·5 per cent, as compared with $\pm$ 0·75 per cent for the working-section of the tunnel when completely empty. The variation in main-stream total head both between and outside the end-plates was negligible.

* Larger extents above and below the chord-line, *e.g.*, right up to the tunnel walls, introduced problems associated with compartmentation of the tunnel working-section. A larger extent upstream of the leading-edge leads to thicker boundary layers (on the end-plates), which can be particularly objectionable with models of small geometric aspect ratio.

† *See* Fig. 2a of Ref 4. The effective aspect ratio could have been increased further by adding lifting surfaces (*e.g.*, large rotatable fairings) between the end-plates and tunnel walls. This was difficult to arrange and inconvenient for the present tests.

‡ Owing to the shortness of the working-section the static of the datum pitot-static tube located in the working-section ahead of the model was affected appreciably by the presence of the model.

2.2. *Blowing Duct and Slot.*—The blowing duct consisted of a simple cylindrical brass tube (external diameter 1·71 in.), which formed the nose of the trailing-edge flap, the air being fed in from both ends of the model. The blowing slot was constructed by cutting a longitudinal slit in the brass tube, and inserting a metal plate (shaped at one end) to form the lower lip of the slot and the top surface of the flap, as shown in Fig. 3. Tie-rods were fixed across the tube to prevent distortion under high pressure, but otherwise no elaboration of the duct proved necessary. Small copper spacers $\frac{1}{16}$th-in. wide were inserted in the blowing slot at spanwise intervals of two inches to maintain spanwise uniformity of slot width.

Before the complete flap was built, extensive bench tests were carried out on a mock-up of the cylindrical duct and slot, including the plate forming the top surface of the flap. The spanwise velocity through the duct was below 50 ft/sec or 100 ft/sec with blowing through both ends or one end respectively, and was of course practically independent of the mass flow for blowing-pressure ratios exceeding that required to choke the blowing slot. Total-head traverses of the jet at distances of 0·1 in. and 0·5 in. behind the slot exit, with blowing pressures of 20 p.s.i. and 40 p.s.i. gauge, exhibited regions of constant high velocity out to about 0·025 in. from the surface. The spanwise variation in the maximum velocity was of the order of $\pm$ 10 per cent except behind the spacers, and could be accredited to difficulties of constructing the small slot widths (0·007 and 0·012 in.) to an accuracy much better than 0·001 in.*. Behind each spacer (0·0625-in. wide) there were wakes of low velocity which extended spanwise as much as 0·4 in. at 0·1 in. behind the slot exit, but then increased little back to 0·5 in. behind the slot. The jet thickness obtained by traverses normal to the plate for the 0·007-in. and 0·012-in. slots were about 0·045 in. and 0·035 in. respectively at a distance 0·1 in. behind the slot exits; by 0·5 in. behind, the jet widths had increased to about 0·095 in. and 0·07 in. respectively. Screw holes countersunk below the top surface of the flap and located 0·3 in. behind the slot exit were filled in, because immediately behind them the peak velocity in the jet was raised about 0·03 in. from the surface, *i.e.* about the same amount as the depth countersunk.

Subsequent total-head traverses on the wind-tunnel model have indicated that the spanwise variations in jet velocity behind the slot become less noticeable with the wind on.

2.3. *Method of Feeding Air to Model.*—Dry, compressed air for blowing was obtained from the High Speed Laboratory storage bottles at a nominal pressure of 350 p.s.i. The arrangement of the external ducting to the model is shown in Fig. 2. A system of two Hale-Hamilton pressure-reducing valves in series was used, together with a subsidiary pressure-controller operating on the dome of the second valve, to give the required blowing pressure at the model and to maintain this pressure automatically when the mains pressure varied between 350 and 150 p.s.i. The air was fed to each end of the model independently, but the ' globe ' valves controlling the air supply to each end were usually left fully open, so that equal amounts of air were then led to both ends. The mass flow fed to the model was determined from measurements of the pressure difference across orifice plates ($1\frac{1}{8}$-in. internal diameter) inserted in straight pipes ($1\frac{3}{4}$-in. internal diameter) in each of the supply lines. The standard relation for the mass flow through the orifice plates[6] was checked on site for the appropriate range of line pressures, by pitot traverses across an auxiliary calibration pipe inserted in the line and also against a rotameter; the error was less than 2 per cent over the whole range. The static pressure on the model side of the orifice plates was registered on a Bourdon dial gauge, which was recalibrated at the lower end of its scale against a mercury U-tube; the static pressure measured at the entry to the model blowing duct was sensibly the same. The temperature of the high-pressure air was also determined, by incorporating a thermo-couple on the model side of the orifice plates, but differed little from that of the tunnel main-stream.

3. *Range of Tests and Reduction of Observations.*—3.1. *Range of Tunnel Experiments.*—Pressure-plotting measurements and tuft observations were made on both the aerofoil and the flap, mostly at a nominal tunnel speed of 100 ft/sec ($R = 1{\cdot}9 \times 10^6$), at wing incidences α

* The slot and duct design has now been slightly modified to reduce this tolerance for future tests.

ranging from $-$ 10 deg to $+$ 20 deg and at flap angles η of 0, 30, 45 and 60 deg. The two blowing-slot widths, $w = 0{\cdot}007$ in. and $0{\cdot}012$ in., were chosen to give a reasonable range of blowing momentum coefficient ($C_\mu = 0$ to $0{\cdot}17$) and blowing-pressure ratios ($p_D/p_0 = 1$ to 5). At the wing incidences of 0 deg and $-$ 10 deg, observations were made at closely spaced intervals of the blowing pressure. At other incidences, observations were made for up to five values of the blowing pressure ratio.

The two blowing-slot positions shown in Fig. 3 were investigated. The slot was first located so that the air was ejected at the intersection ($\phi = 0$ deg) of the round nose of the flap and the straight upper surface of the wedge-shaped trailing-edge. This so-called rear slot was the simplest to make and it was considered that more rearward positions would be relatively ineffective. In the light of experience with area-suction flaps, the slot was later moved further forward to the so-called mid-slot position ($\phi = 30$ deg), half-way round the flap knee when $\eta = 60$ deg., *i.e.*, roughly where the minimum pressure occurs with attached flow*.

The thickness of the slot upper lip on the model was not much more than $0{\cdot}006$ in., *i.e.*, no larger than the slot widths tested. Now, in practice, the lip thickness may need to be several times the slot width from strength considerations. The effect of thickening the upper lip of the model, by sticking on successive layers of Porvic† each $0{\cdot}032$ in. deep and extending 2 in. forward of the slot exit, was therefore investigated. A slightly porous material was essential in order that the covered static-pressure tubes could continue to record the external surface pressure; no difficulties were experienced with up to five layers of Porvic, $0{\cdot}16$ in. thick overall.

The effect of local blockage of the slot on the sectional pressure distribution was also briefly investigated‡. A single half-inch block was first inserted so as to seal up the slot for $\frac{1}{4}$ in. each side of the chordwise line of pressure holes. Next, a further three half-inch blocks were added on each side, spaced so as to leave regular half-inch gaps between the blocks. Later, these blocks were shifted spanwise so that the pressure holes were in-line with the middle of a gap instead of the middle of a block. Finally, the experiments were repeated using blocks and gaps 1 in. wide.

3.2. *Reduction of Surface Pressure Measurements.*—The sectional lift and pitching-moment forces were derived by chordwise integration of the surface static pressures. The static holes in the model were sufficiently regular and numerous (*see* Fig. 4) to permit the use of a simple numerical method of integration. The main-stream dynamic head was taken as that recorded by a standard pitot-static inserted midway between the end-plates in the aerofoil $\frac{1}{4}$-chord position with the model removed but all other parts of the rig in place. This value was also subsequently confirmed by flow explorations about the model and a comparison of measured and theoretical surface-pressure distributions at zero lift with the flap undeflected. No further corrections were applied to allow for tunnel constraint and blockage effects, since the validity of conventional formulae is doubtful for the present set-up, particularly under high lift conditions. The pressure coefficient C_p corresponding to a surface static pressure p measured on the aerofoil surface was evaluated using the relation $(1 - C_p) = (H_0 - p)/\frac{1}{2}\rho_0 U_0^2$, since the variation in the main-stream total head H_0 was found to be negligible over the working-section.

3.3. *Evaluation of Blowing Coefficients.*—The blowing momentum coefficient is defined as

$$C_\mu = \frac{Mv_j}{\frac{1}{2}\rho_0 U_0^2 S'} = 2C_Q \frac{v_j}{U_0}.$$

The blowing quantity coefficient $C_Q[= M/\rho_0 U_0 S']$ was evaluated from orifice-plate measurements of the mass flow supplied to the model. The blowing velocity v_j was determined theoretically, assuming isentropic expansion of the ejected air from the duct (stagnation) pressure p_D to the main-stream static pressure p_0, as in Ref. 1.

* Tests are also to be made with a third slot position, even further forward ($\phi = 60$ deg), to simulate blowing from the shroud at $\eta = 60$ deg, and to investigate the effectiveness of flap blowing at flap angles of 90 deg and beyond.

† A micro-porous plastic material used for accumulator separators.

‡ The effect on the overall lift of the wing could not be examined since the model had pressure holes at only one spanwise station.

Now, the ratio v_j/a_D of the blowing velocity to the velocity of sound in the duct is purely a function of the blowing pressure ratio p_D/p_0, since

$$\frac{v_j}{a_D} = \left(\frac{2}{\gamma - 1}\right)^{1/2} \left\{1 - \left(\frac{p_0}{p_D}\right)^{(\gamma-1)/\gamma}\right\}^{1/2}.$$

Moreover,

$$\frac{v_j}{U_0} \equiv \left(\frac{v_j}{a_D}\right)\left(\frac{U_0}{a_D}\right)^{-1} = \left(\frac{v_j}{a_D}\right)\left(\frac{U_0}{a_0}\right)^{-1}\left(\frac{T_D}{T_0}\right)^{1/2}$$

is also dependent only on main-stream and duct conditions, *i.e.*, is independent of slot width. Both these velocity ratios† are plotted in Fig. 5 and listed in Table 1 at regular intervals of p_D/p_0. In our experiments the difference between T_D and T_0, the duct and main-stream temperatures, was negligible; hence, the difference between a_D and a_0 could likewise be ignored.

Theoretical (isentropic flow) values for C_Q can also be evaluated for a known slot area A_t. For supersonic blowing through a choked slot, i.e., $p_D/p_0 > \{(\gamma + 1)/2\}^{\gamma/(\gamma-1)}$, we have

$$C_Q = \frac{1}{\rho_0 U_0}\frac{A_t}{S'}\left\{\frac{\gamma}{\mathscr{R}}\left(\frac{2}{\gamma+1}\right)^{\frac{\gamma+1}{\gamma-1}}\right\}^{1/2}\frac{p_D}{T_D^{1/2}}$$

$$= \left(\frac{U_0}{a_0}\right)^{-1}\frac{A_t}{S'}\left(\frac{T_0}{T_D}\right)^{1/2}\left\{\frac{2}{(\gamma+1)}\right\}^{\frac{\gamma+1}{2(\gamma-1)}}\frac{p_D}{p_0}.$$

For subsonic blowing, i.e., $p_D/p_0 < \{(\gamma + 1)/2\}^{\gamma/(\gamma-1)}$,

$$C_Q = \frac{1}{\rho_0 U_0}\frac{A_t}{S'}\left\{\frac{\gamma}{\mathscr{R}}\frac{2}{\gamma-1}\right\}^{1/2}\left(\frac{p_0}{p_D}\right)^{1/\gamma}\left\{1 - \left(\frac{p_0}{p_D}\right)^{\frac{\gamma-1}{\gamma}}\right\}^{1/2}\frac{p_D}{T_D^{1/2}}$$

$$= \left(\frac{U_0}{a_0}\right)^{-1}\frac{A_t}{S'}\left(\frac{T_0}{T_D}\right)^{1/2}\left\{\frac{2}{\gamma-1}\right\}^{1/2}\left(\frac{p_D}{p_0}\right)^{\frac{\gamma-1}{\gamma}}\left\{1 - \left(\frac{p_0}{p_D}\right)^{\frac{\gamma-1}{\gamma}}\right\}^{1/2}.$$

Theoretical values of both C_Q and C_μ are listed at regular intervals of p_D/p_0 in Table 1 for general reference. They are quoted for the representative test conditions $U_0 = 100$ ft/sec, $A_t/S' = 4 \times 10^{-4}$ (larger slot width), and with $a_0 = 1117$ ft/sec, $T_D = T_0$, with $\gamma = 1{\cdot}4$. The procedure for scaling to other conditions is also indicated.

The experimental C_Q values were found to be about 10 per cent lower than the corresponding theoretical values, but this difference can be partly ascribed to errors in the measured slot area A_t (inserted in the theoretical relations) as well as to neglecting viscous effects in the theory.

4. *Lift Results.*—4.1. *Lift at Constant Incidence.*—The C_L vs. C_μ curves at zero incidence with flap angles η of 30 deg and 45 deg are given in Fig. 6a for blowing through the small rear slot ($\phi = 0$ deg, $w_t/c = 0{\cdot}0002$). As expected[1], the lift rises rapidly with increasing C_μ until flow separation on the flap is completely prevented (boundary-layer control). Thereafter, the lift still rises (supercirculation) but at a much lower rate comparable with jet flap schemes[4]. For $\eta = 45$ deg and above, blowing through the small rear slot is completely ineffective below $C_\mu = 0{\cdot}01$, even though the blowing velocity is well above the main-stream velocity. This ineffectiveness at low C_μ values together with the poor results achieved with blowing for $\eta = 60$ deg (*see* later) could be attributed to the far-back position of the slot.

† The ratio v_j/U_0 is presented for the representative conditions $U_0 = 100$ ft/sec, $a_0 = 1117$ ft/sec, $T_D = T_0$, with $\gamma = 1{\cdot}4$; the procedure for scaling to other conditions is also indicated.

As in Ref. 1, a datum lift increment

$$\Delta C_{L\,t} = a_1 \,.\, \lambda_1 \,.\, \eta \quad .. \quad .. \quad .. \quad .. \quad .. \quad .. \quad (1)$$

given by linearised thin-aerofoil theory is marked on the curves. This provides a simple measure of the lift increment obtainable by flap deflection when flow separation is prevented, and the corresponding C_μ value gives a useful indication of the efficiency of blowing. For our purposes the value of the lift-curve slope a_1 is taken as that for the unflapped aerofoil (without blowing) well below the stall, namely, 0·068/deg, and λ_1 is assigned the value 0·61 given by Glauert's mean-line theory when $c_f/c = 0{\cdot}25$. A more elaborate but less convenient estimate could be derived from the non-linear lift-incidence relation

$$C_L = a_1 \sin(\alpha + \beta) \,, \quad .. \quad .. \quad .. \quad .. \quad .. \quad (2)$$

together with Keune's exact mean-line theory which takes into account the effect of flap deflection on a_1 as well as on the no-lift angle $(-\beta)$*.

The points on the C_L vs. C_μ curves (Fig. 6a), which satisfy the relation (1), are seen to lie where the rate of increase of C_L with C_μ begins to fall off markedly. C_μ values of only 0·014 and 0·034 sufficed to produce the appropriate values of $\Delta C_{L\,t}$ for $\eta = 30$ deg and 45 deg respectively at zero wing incidence.

Since, even at zero incidence, a small bubble of separated flow occurred on the nose of this aerofoil with the trailing-edge flap deflected, some C_L vs. C_μ curves corresponding to $\alpha = -10$ deg have also been included. The shape of the curve for $\eta = 45$ deg (*see* Fig. 6b) is not much different from that at zero incidence, except at extremely small C_μ values, nor are the lift increments due to blowing and the value of C_μ required to provide the theoretical lift increment $\Delta C_{L\,t}$.

The effect of increasing the slot width to $w_t/c = 0{\cdot}00033$ is shown by comparing Figs. 7a and 7b with Figs. 6a and 6b. Particularly at $\alpha = -10$ deg, there is no great change in the C_L vs. C_μ curves for $\eta = 30$ deg and 45 deg except perhaps at very low C_μ values, so that the correlation of lift results on a C_μ basis seems justified. The C_μ value required to provide the total lift increment $\Delta C_{L\,t}$ for $\eta = 45$ deg at $\alpha = 0$ deg rises from 0·034 to 0·043 with the increase in slot width.

The C_L vs. C_μ curves for $\eta = 60$ deg at both incidences are not of the normal shape, and the C_μ value for $\Delta C_{L\,t}$ is unduly high, being above 0·15. At this large flap angle, the rear slot position ($\phi = 0$) was located too far back for the induced flow due to blowing to control effectively the separation on the flap knee upstream of the blowing slot. The C_L vs. C_μ curves obtained with the slot moved forward to the ' mid-slot ' position ($\phi = 30$ deg in Fig. 3), about half-way round the flap knee, are shown in Figs. 8a and 8b for $\alpha = 0$ and -10 deg respectively and $w_t/c = 0{\cdot}00033$. The improvement in the effectiveness of blowing is remarkable for $\eta = 60$ deg; *e.g.*, the C_μ value required to produce the appropriate $\Delta C_{L\,t}$ is only about 0·07. There is also some improvement for $\eta = 45$ deg, the required C_μ value being about 0·028. Unfortunately, flap angles above 60 deg could not be tested with the present arrangement, but modifications to permit such tests with a slot position even further forward ($\phi = 60$ deg) are in hand.

Only a few experiments were made with the small mid-slot ($\phi = 30$ deg, $w_t/c = 0{\cdot}0002$), as the model was in this instance not entirely satisfactory because of inadequate sealing of screwed fittings in the duct. Nevertheless, the lift results obtained were closely similar to those for the large mid-slot at corresponding C_μ values.

The values of C_μ required to produce the theoretical lift increments $\Delta C_{L\,t}$ in the present quasi two-dimensional tests are only about half the corresponding values in earlier two-dimensional tests with subsonic and supersonic blowing from the shroud over the trailing-edge flap[1]. However, they are much the same as those needed in current N.P.L. tests with blowing from the

* On this theory, for $c_f/c = 0{\cdot}25$ and $\eta = 60$ deg, the change in no-lift angle due to flap deflection is only 1 per cent less than the value $\lambda_1\eta$ predicted by Glauert's linear theory, but the lift-curve slope a_1 is reduced by 4½ per cent. Use of the non-linear relation (2) instead of (1) to give the lift increment at $\alpha = 0$ deg leads also to a further reduction of 6 per cent in lift. For $\eta = 45$ deg, the respective decreases are 1, 2½ and 3½ per cent.

shroud on a 60 deg delta model. Consequently, the low C_μ values may be partly associated with aspect-ratio effects, as well as with blowing from the flap itself or other improvements in technique. This is not surprising since, for a prescribed change in sectional no-lift angle due to flap deflection, the resulting adverse velocity gradients over the aerofoil section will in general increase with the lift-incidence curve slope, *i.e.*, with the effective aspect ratio. It is also significant that the lift increment due to flap deflection without blowing is a greater proportion of the theoretical ΔC_{L_t} in the present test (effective aspect ratio 3·3) than in the earlier two-dimensional tests.

4.2. *Variation of Lift with Incidence.*—Lift-incidence curves for a range of C_μ values with the small rear slot ($w_t/c = 0{\cdot}0002$, $\phi = 0$) are shown in Figs. 9a and 9b for $\eta = 30$ deg and 45 deg respectively, together with the curve for the plain aerofoil ($\eta = C_\mu = 0$). The stalling incidence ($dC_L/d\alpha = 0$) is seen to be about 15 deg for the plain aerofoil and becomes some 3 deg and 5 deg less respectively when $\eta = 30$ deg and 45 deg without blowing. There are further reductions of similar magnitudes when a moderate amount of blowing is applied ($C_\mu \doteq 0{\cdot}03$) just sufficient to prevent flow separation over the flap at zero wing incidence. For higher rates of blowing, there is no further reduction and in some cases there is even a slight recovery of stalling angle. The increment in maximum lift $\Delta C_{L\,\max}$ resulting from flap deflection and blowing is plotted against C_μ in Fig. 12, and is of the order of two-thirds the corresponding lift increment ΔC_L at zero incidence shown in Fig. 6a.

The lift-incidence curve for the plain aerofoil remains substantially linear up to $\alpha = 10$ deg, where there is a change in slope associated with the change in the characteristics of the laminar separation bubble at the wing nose (*see* Section 6.1). The value of $dC_L/d\alpha$ at low incidences is 0·068/deg which agrees well with values from two-dimensional aerofoil data corrected to allow for the effective aspect ratio 3·3 of the present model between end-plates. When the flap is deflected without blowing, the lift-incidence curves are not usually linear except at appreciable negative incidence. This is not surprising in view of the complex flow separation pattern on the wing upper surface, which at low incidence consists of a laminar separation bubble at the nose followed by a region of turbulent attached flow and finally turbulent boundary-layer separation at the flap knee (*see* Section 6.1). The linearity of the lift-incidence curves below the stall is much improved, however, by moderate amounts of blowing (*see* Fig. 9b), sufficient to prevent flow separation on the flap. The value of $dC_L/d\alpha$ becomes much the same as for the unflapped aerofoil and tends to rise slightly with greater rates of blowing.

Figs. 10 and 11 give the lift-incidence curves for the larger rear slot ($w_t/c = 0{\cdot}00033$, $\phi = 0$) and for the larger mid-slot ($w_t/c = 0{\cdot}00033$, $\phi = 30$ deg) respectively. The corresponding curves of $\Delta C_{L\,\max}$ against C_μ are included in Fig. 12. The change in slot width made no significant difference to the effectiveness of blowing at a given C_μ. The forward movement of the slot position yielded only slightly better results with $\eta = 30$ and 45 deg, but for $\eta = 60$ deg the improvement was remarkable as already mentioned in Section 4.1.

With powerful trailing-edge flaps on thin straight wings as considered here, the wing lift ceases to increase with incidence at quite small angles. The application of boundary-layer control at the wing nose, to increase lift by raising the stalling incidence, is therefore particularly attractive since the penalty of abnormally high wing incidence is not encountered. Experiments are to be made on the present aerofoil with blowing from the knee of a simple leading-edge flap (hinged nose). For thin aerofoils, this scheme should be much more effective than blowing close to the leading edge without deflecting the nose.

4.3. *Effect of Increased Slot Lip Thickness.*—Fig. 13 demonstrates that thickening the upper lip of the large rear slot decreased the lift produced with $\eta = 45$ deg at constant values of α and C_μ. With $\alpha = -10$ deg and $C_\mu = 0{\cdot}03$, the lift falls little at first below that for the unthickened lip, *e.g.*, the C_L value is reduced by only 0·02 when the total slot lip thickness l reaches 0·038 in. ($l/w_t \doteq 3$), but then decreases steadily, so that when l reaches 0·166 in. ($l/w_t \doteq 14$) the C_L value is reduced by about 0·25. At the same negative incidence, but with the higher C_μ value of 0·058, the trend is the same, though the reduction in C_L is slightly smaller. At zero incidence, which is

only a few degrees below the wing stall, the C_L value decreases more quickly with increasing lip thickness right from the start; the reduction in C_L for $l = 0{\cdot}166$ in. is about $0{\cdot}3$ with $C_\mu = 0{\cdot}03$ and again slightly less for the higher C_μ. Since the largest lip thickness was only about one-third the thickness of the turbulent boundary layer just ahead of the curved nose of the flap, lip thickening probably had no significant effect on the boundary layer ahead of the separation point. On the other hand, under still-air conditions, the jet thickness would only reach the value $l = 0{\cdot}166$ in. about 1 in. distance behind the exit, *i.e.*, more than 3 per cent chord downstream of the separation point on the flap knee.

4.4. *Effect of Local Slot Blockage.*—Fig. 14 gives a few results on the effect of local slot blockage on the sectional lift coefficient, plotted as a function of the C_μ value for the aerofoil as a whole*; they refer to blowing through the large rear slot with $\alpha = 0$ and $\eta = 45$ deg. A single block (spacer) of half-inch width led to no significant reduction in the sectional lift increment obtained at moderate C_μ values ($\simeq 0{\cdot}03$). Moreover, the addition of three half-inch blocks each side of the pressure holes, spaced so as to leave regular half-inch gaps, reduced the sectional lift coefficient less than $0{\cdot}1$ for $C_\mu \geqslant 0{\cdot}05$. Similar experiments with one-inch blocks, however, increased the losses in sectional lift coefficient to $0{\cdot}25$ or more.

A more elaborate investigation of the effect of slot blockage on both the sectional lift and overall wing lift coefficients will be possible by pressure-plotting and balance measurements now being carried out on a 60 deg delta-wing model.

5. *Pitching-Moment Results.*—Fig. 15 gives curves of pitching moment C_m about the quarter-chord point plotted against lift C_L for $\eta = 30$ and 45 deg, with blowing through the small rear slot at constant C_μ and varying α, and *vice versa*. The C_m vs. C_L curve for the plain aerofoil is included for comparison, and is typical for thin aerofoils exhibiting both short and long (expanding) separation bubbles through the incidence range[7]. The curve is reasonably straight and the aerodynamic centre moves little away from the quarter-chord point below $C_L = 0{\cdot}5$ ($\alpha = 8$ deg), while the stall is both gentle and stable (*see* Fig. 15). When the flap is deflected, the curve is as usual moved bodily downwards to more negative C_m values, and tends to become more non-linear. The stall occurs at a lower incidence (but higher lift) than for the plain aerofoil and remains stable. When sufficient blowing is applied to prevent flow separation on the flap, the C_m vs. C_L curves (C_μ constant, α varying) are displaced to even more negative C_m values, but become reasonably straight again below the stall; the stall occurs still earlier and becomes unstable.

The C_m vs. C_L curves at constant incidence, with C_μ varied, are in general straight and parallel. For $\eta = 30$ deg, they also pass through the corresponding points for the plain aerofoil ($\eta = C_\mu = 0$). The ratio $-\Delta C_m/\Delta C_L$ of the increment in nose-down pitching moment to the lift increment produced by flap deflection and blowing is therefore sensibly constant at about $0{\cdot}25$, so that the centre of pressure remains close to the half-chord point. For $\eta = 45$ deg, the value of $(-\Delta C_m/\Delta C_L)$ is only $0{\cdot}23$ without blowing, but rises again to about $0{\cdot}25$ when blowing is applied. These values are somewhat larger then $0{\cdot}17$, the result predicted by linearised theory, but agree well with the results of German tests with subsonic blowing from the wing shroud over the trailing-edge flap on a 9 per cent thick wing section[1]. The difference between experiment and theory could partly be accounted for by the nose-separation characteristics of thin sections.

The pitching-moment curves for the large rear slot (Fig. 16) and the values of $-\Delta C_m/\Delta C_L$ are in general similar to those just discussed; a difference occurs in the C_m vs. C_L curves for the flap deflected without blowing, over the negative incidence range. The curves for the mid-slot position are again little changed for $\eta = 30$ and 45 deg (Fig. 17). For $\eta = 60$ deg, the value of $-\Delta C_m/\Delta C_L$ without blowing is only $0{\cdot}2$, but it again rises to about $0{\cdot}25$ with moderate amounts of blowing.

* This is as usual based on the measured mass flow fed to the aerofoil, the theoretical blowing velocity for isentropic flow, and the boundary-layer control area S' of the wing corresponding to the spanwise extent of the whole slot. The sectional C_μ value at the open areas of the slot is slightly higher, in the ratio of the old unblocked slot area to the new slot area.

6. *Flow Characteristics and Pressure Distributions.*—6.1. *Development of Separated Flow Regions.*—For the plain aerofoil, tuft observations indicated smooth flow over the upper surface of the aerofoil up to 9 deg incidence. Both the pressure distributions (Fig. 18) and china clay observations confirmed that the laminar separation bubble was contained within the first 2 per cent chord. As the incidence was raised beyond 9 deg, the tufts showed separation close to the leading-edge with the position of turbulent reattachment moving steadily rearwards. At incidences of 12 and 15 deg, the separation bubble extended back to about mid-chord and the trailing-edge respectively.

For flap deflections of 30 deg or more, without blowing, the flow over the trailing-edge flap was completely separated at all the aerofoil incidences tested. The behaviour of the separation bubble on the aerofoil nose with variation of incidence was similar to that for the plain aerofoil, except that the incidences at which the bubble began to expand or at which separated flow extended right back to the trailing-edge were some 3, 4 and 5 deg less with 30, 45 and 60 deg respectively. These decreases occurred because, at a given incidence, the adverse pressure gradients over the aerofoil nose became steeper with the increased circulation arising from flap deflection. It will be recalled from Section 4.2 that the stalling incidences ($dC_L/d\alpha = 0$) were also reduced by roughly these amounts due to flap deflection.

With moderate amounts of blowing, the nose bubble began to expand at incidences up to 2 deg earlier than without blowing, depending on the flap deflection. When the C_μ value was increased much more, say by 0·1 to produce supercirculation, this incidence was reduced further by up to 2 deg. However, the incidence at which the nose bubble extended back to the flap knee seemed hardly affected by blowing, in contrast to the reduction of stalling incidence caused by moderate amounts of blowing (*see* Section 4.2). Widening the slot had little upstream influence on the development of the nose bubble, nor had forward movement of the slot position apart from reducing the C_μ value needed to control the flow separation on the flap.

6.2. *Pressure Distributions.*—The variation of pressure distribution with incidence for the plain aerofoil is shown in Fig. 18. As the incidence is raised beyond 10 deg, the region of fairly constant pressure over the front of the laminar separation bubble at the aerofoil nose extends steadily rearwards, while the maximum suction ($-C_p$) falls instead of rising with incidence. The value of $-C_p$ at the wing trailing-edge simultaneously rises (lower pressure, higher velocity), owing to thickening of the turbulent boundary-layer at the trailing-edge, followed eventually by complete separation.

Some representative pressure distributions to illustrate the effect of flap deflection and blowing are given in Fig. 19a for $\alpha = 0$ and $\eta = 45$ deg, with various rates of blowing through the small rear slot. Without blowing, the peak suction developed on the flap is only small ($-C_p = 1{\cdot}3$) and is located right at the beginning of the curved flap knee (hole 16 in Fig. 4). There is a slight recovery of pressure over the knee, but thereafter the value of $-C_p$ remains constant and positive indicating completely separated flow over the rest of the flap. As the blowing momentum increases from zero, the peak suction on the flap knee increases and is located slightly further rearward, while the extent of the constant pressure (separated flow) region decreases. Simultaneously the peak suction at the aerofoil nose also rises above the value $-C_p = 1{\cdot}7$ achieved without blowing, but to a much smaller degree than that at the flap knee, partly because there is no form of boundary-layer control to prevent separation at the aerofoil nose, and partly because the aerofoil is strictly not two-dimensional, so that three-dimensional downwash effects reduce the nose peak at mid-span. For example, with $C_\mu = 0{\cdot}029$, the values of the peak suctions at the flap knee and aerofoil nose respectively are $-C_p = 7{\cdot}4$ and $3{\cdot}6$. The peak on the flap has then moved back about half-way round the curved knee (hole 18). There is no constant pressure region on the flap upper surface, and $-C_p = -0{\cdot}3$ at the trailing-edge, thus implying that separation is completely prevented on the flap. When the C_μ value is increased further to 0·51, so that supercirculation above that corresponding to attached flow is produced, the values of $-C_p$ rise only to $8{\cdot}2$ and $4{\cdot}3$ at the flap knee and aerofoil nose respectively, while at the trailing-edge $-C_p$ falls only to $-0{\cdot}35$. Fig. 19b shows a similar range of pressure distributions

for blowing through the large mid-slot at zero wing incidence. In this case small undulations appeared in the pressure recovery from the minimum on the flap knee to the trailing-edge pressure when the C_μ values were large enough to produce supercirculation.

In order to provide some idea of the variation of the pressure distribution with incidence and flap angle as well as blowing (without recourse to numerous graphs), the peak suctions measured at the aerofoil nose and the flap knee have been plotted against α in Figs. 20 and 21, together with the trailing-edge pressure, for $\eta = 30$, 45 and 60 deg with blowing through the large mid-slot. The incidence at which the largest nose peak suction is reached (Fig. 20) is practically the same as that at which the nose bubble begins to expand (*see* Section 6.1). For a fixed C_μ, the peak suction on the flap knee and the trailing-edge pressure (Fig. 21), remain fairly constant as the incidence is first increased, but eventually the flap peak suction begins to fall rapidly. Simultaneously the trailing-edge pressure diverges from its small constant value ($-C_p$ negative) towards its value without blowing ($-C_p$ positive), though this change is somewhat delayed at high blowing pressures corresponding to supercirculation. Comparison of the curves in Figs. 20 and 21 suggests that blowing over the flap becomes less effective as the separation bubble on the aerofoil nose expands.

6.3. *C_μ Values to Prevent Flow Separation on Flap.*—The minimum amount of blowing needed to produce attached flow over the flap is difficult to estimate precisely because observations were not made at enough C_μ values over the lower end of the range*. Because the flow over the flap is usually highly turbulent, a better indication of attached flow than tuft studies is probably the development of a small positive trailing-edge pressure ($-C_p$ negative) accompanied by a large peak suction at the flap knee, as discussed in Section 6.2. This is further illustrated by Fig. 22 where the variation of the flap peak suction and the trailing-edge pressure with C_μ is plotted at constant incidence.

For the small rear slot, the C_μ values needed to ensure attached flow on the flap with $\eta = 30$ and 45 deg did not exceed 0·02 at small or negative incidences. However, as already commented in Section 6.2, the value increased appreciably with incidence once the separation bubble at the aerofoil nose began to expand, *i.e.*, when the thickness of the turbulent boundary layer just ahead of the blowing slot rapidly increased. For example, the required C_μ value was more than doubled when α increased from 0 to 5 deg, *i.e.*, when the nose bubble spread back to 20 per cent chord. With $\eta = 60$ deg, a C_μ value of 0·15 was needed even at $\alpha = 0$ deg.

Forward movement of the slot did not lead to much improvement in the C_μ values for $\eta = 30$ and 45 deg. However, for $\eta = 60$ deg, the C_μ values required at incidences of 2 deg and below were not more than 0·04 with the mid-slot, a large improvement indeed. As the incidence was raised above 2 deg, and the nose bubble expanded, the C_μ for $\eta = 60$ deg with blowing through the mid-slot steadily increased to the large value needed with the rear slot.

In general, the blowing momentum required at zero incidence to prevent flow separation on the flap was slightly lower than that required to produce the linear theoretical lift increment $\Delta C_{L\,t}$ due to flap deflection with blowing. This is to be expected since the linear theory tends to overestimate the lift increment for unseparated flow at large flap angles (*see* Section 4.1).

7. *General Conclusions.*—The blowing momentum coefficient proved to be a reasonably satisfactory parameter for correlating the lift increments obtained with the two slot widths ($w_t/c \simeq 0{\cdot}0002$ and 0·00033), over the normal practical range of C_μ (0 to 0·15) and pressure ratio ($p_D/p_0 = 1$ to 5). This agrees with the David-Taylor Model-Basin supersonic blowing results[3]†.

Blowing through the rear slot, located at the intersection of the round nose of the flap and the straight upper surface of the wedge-shaped trailing edge, was quite effective for flap angles up to 45 deg, but not for $\eta = 60$ deg. Movement of the slot forward to about half-way round the

* The C_μ values required were much lower than originally envisaged.

† The correlation of earlier German subsonic blowing results[1] on a C_μ basis was far from satisfactory but was nevertheless superior to correlation in terms of C_Q.

flap knee when $\eta = 60$ deg, *i.e.*, roughly at the peak suction for attached flow, led to a remarkable improvement with $\eta = 60$ deg, and a slight improvement with $\eta = 45$ deg. Tests are in hand with another slot position further forward still, primarily to investigate the effectiveness of blowing at flap angles of 90 deg and beyond, but also to simulate blowing from the shroud with $\eta = 60$ deg.

The C_μ values needed to give the lift increment $\Delta C_{L\,t}$ predicted by linear theory for unseparated flow[1], as defined by equation (1), were 0·014, 0·028 and 0·07 when $\eta = 30$, 45 and 60 deg respectively, with the aerofoil at zero incidence and blowing at the mid-slot position. The corresponding values needed to ensure attached flow on the flap were slightly lower, as expected. These C_μ requirements are considerably less than those of earlier two-dimensional tests[1, 3]. However, a considerable part of the reduction may well be associated with the low effective aspect ratio (lift-incidence curve slope) of the present quasi two-dimensional model, as well as with the improvements in blowing techniques.

The increments in maximum lift due to flap deflection with blowing were only about two-thirds the corresponding lift increments at zero incidence, because of the reduction in stalling angle. With high rates of blowing, however, the stalling angle tended to increase again and the lift-curve slope began to rise above that for the unflapped aerofoil. The separation bubble on the aerofoil nose began to expand when the incidence reached only a few degrees and simultaneously the blowing momentum needed to prevent flow separation on the flap tended to rise.

An increase in the ratio of slot lip thickness to slot width, from below unity to a normal full-scale value (say 3), caused only a small reduction in the lift increment due to blowing, but higher ratios seem undesirable. A single spacer up to half-inch wide had a negligible effect on the sectional lift coefficient in the vicinity. Moreover, the reduction of sectional lift from the addition of a further three spacers on each side, half-inch wide and with regular half-inch gaps between, was less than that due to the presence of a single spacer one-inch wide.

The chordwise position of the centre of pressure moved steadily rearward with both flap deflection and blowing. The ratio $-\Delta C_m/\Delta C_L$ due to flap deflection without blowing was 0·25 for $\eta = 30$ deg, but fell to 0·2 when $\eta = 60$ deg. However, with blowing, the ratio quickly rose again to 0·25 at all flap angles.

The pressure distributions discussed in Section 6.2 illustrate the variation of chordwise loading on the aerofoil with incidence, flap angle and blowing. Moreover, the values of the pressure minima on the aerofoil nose and the flap knee, together with the trailing-edge pressure, give a useful indication of the development and suppression (by blowing) of the separated flow regions. Boundary-layer explorations on the upper surface of the flap and some wake-drag measurements will be reported separately.

From a purely practical standpoint, the present experiments clearly demonstrate that a satisfactory spanwise distribution of blowing slot velocity can be achieved with the simplest cylindrical duct, provided the duct velocity is not much greater than say one-tenth the slot velocity. For supersonic blowing, the loss in pressure down such a duct is relatively insignificant compared with the mean duct pressure. The analysis of lift results shows that, at least for low aspect-ratio wings, much smaller C_μ values than hitherto envisaged are required to ensure that the flap gives the theoretical lift increment at low wing incidences. However, it is obvious that the benefits of such powerful trailing-edge flaps cannot be enjoyed to the full on thin wings, unless boundary-layer control is simultaneously applied at the wing nose, so that positive wing incidence still remains an effective and usable method of producing lift. For this reason, experiments with blowing at the wing nose are being carried out in conjunction with the further work on trailing-edge flap blowing and on jet flaps.

8. *Acknowledgements.*—The computational and graphical work associated with the reduction of observations was carried out by Miss E. M. Love and Miss L. M. Esson. Miss A. K. Kernaghan assisted with some of the experimental work. The model was designed by Mr. N. Marcus and was built in the Aerodynamics Division Workshop.

LIST OF SYMBOLS

a		Speed of sound
a_1		Slope of lift-incidence curve
	$=$	$dC_L/d\alpha$
A_t		Throat area of blowing slot
c		Aerofoil chord
c_f		Flap chord
C_L C_m		Lift and pitching-moment coefficients (about $\frac{1}{4}$-chord) obtained by chordwise integration of surface static pressures measured at the mid-span station
ΔC_L, ΔC_m		Increments in C_L and C_m due to combined flap deflection and blowing
ΔC_{Lt}		Datum lift increment given by linearised theory
	$=$	$a_1 \cdot \lambda_1 \cdot \eta$; *see* Section 4.1
C_Q		Blowing-quantity coefficient
	$=$	$M/\rho_0 U_0 S'$
C_μ		Blowing-momentum coefficient
	$=$	$Mv_j/\frac{1}{2}\rho_0 U_0^2 S'$
C_p		Surface static-pressure coefficient
	$=$	$(p - p_0)/\frac{1}{2}\rho_0 U_0^2$
	$=$	$1 - (H_0 - p)/\frac{1}{2}\rho_0 U_0^2$
l		Thickness of slot upper lip
M		Mass flow (slugs/sec) of blowing air fed to model
p		Surface static pressure
p_0, H_0, ρ_0, U_0, T_0		Main-stream static pressure, total head, density, velocity, and temperature
p_D, ρ_D, T_D		Blowing duct (stagnation) pressure, density and temperature
R		Main-stream Reynolds number
	$=$	$U_0 c/\nu$
$\mathscr{R}$		Universal gas constant
S'		Wing plan-form area corresponding to spanwise extent of boundary-layer control
v_j		Blowing velocity assuming isentropic expansion from the duct to main-stream pressure (*see* Section 3.3)
w_t		Slot throat width; $w_t/c = A_t/S'$ for uniform unblocked slot on a two-dimensional model
x		Chordwise distance aft of aerofoil leading edge
α		Aerofoil incidence
$-\beta$		No-lift angle
γ		Ratio of specific heats $= 1{\cdot}4$ for air
ϕ		Angle defining slot position on flap knee (*see* Fig. 3)
η		Trailing-edge flap angle relative to aerofoil chord-line

REFERENCES

No.	*Author*	*Title, etc.*
1	J. Williams	An analysis of data on blowing over trailing-edge flaps for increasing lift. C.P. 209. September, 1954.
2	J. S. Attinello	An interim attack airplane from a Navy fighter. Bu. Aer. Report DR–1417. July, 1952.
3	E. L. Harkleroad and D. R. Murphy	Two-dimensional tests of a model of an F9F–5 airplane wing section using a high-speed jet blowing over the flap. Part I—Tests of a 6 ft chord model. D.T.M.B. (U.S. Navy) Rep. Aero. 845. 1953.
4	J. Williams and A. J. Alexander ..	Three-dimensional wind-tunnel tests of a 30 deg jet-flap model. C.P.304. November, 1955.
5	W. Mangler and J. Rotta	Theory of the three-dimensional areofoil. Part I—Theory of the supporting line. AVA Monograph F_1 M.o.S. R. & T. 1023. A.R.C. 11,553. F.M. 1253. November, 1947.
6	R. C. Pankhurst and D. W. Holder	*Wind-Tunnel Technique.* Pitmans. 1952
7	G. B. McCullough and D. E. Gault	Examples of three representative types of airfoil section stall at low speed. N.A.C.A. Tech. Note 2502. September, 1951.

TABLE 1

Standard Table for Blowing Parameters

$\frac{p_D}{p_0}$	$\frac{v_j}{a_D}$	$\frac{v_j^*}{U_0}$	C_Q^*	C_μ^*
1·0	0	0	0	0
1·1	0·3665	4·094	0·00168	0·0138
1·2	0·5038	5·627	0·00237	0·0267
1·3	0·6009	6·712	0·00289	0·0388
1·4	0·6770	7·562	0·00333	0·0504
1·5	0·7396	8·261	0·00371	0·0613
1·6	0·7927	8·854	0·00405	0·0717
1·7	0·8387	9·368	0·00436	0·0817
1·8	0·8792	9·821	0·00465	0·0913
1·9	0·9153	10·224	0·00491	0·1005
2·0	0·9478	10·587	0·00517	0·1095
2·2	1·0042	11·217	0·00569	0·1276
2·4	1·0519	11·750	0·00621	0·1458
2·6	1·0930	12·208	0·00672	0·1641
2·8	1·1288	12·609	0·00724	0·1826
3·0	1·1606	12·964	0·00776	0·2011
3·2	1·1890	13·281	0·00827	0·2198
3·4	1·2146	13·567	0·00879	0·2385
3·6	1·2379	13·827	0·00931	0·2574
3·8	1·2592	14·065	0·00983	0·2764
4·0	1·2788	14·284	0·01034	0·2955
4·5	1·3216	14·762	0·01164	0·3435
5·0	1·3576	15·164	0·01293	0·3921
5·5	1·3885	15·509	0·01422	0·4411
6·0	1·4154	15·810	0·01551	0·4905
6·5	1·4391	16·075	0·01681	0·5403
7·0	1·4603	16·311	0·01810	0·5905
7·5	1·4793	16·524	0·01939	0·6409
8·0	1·4966	16·717	0·02069	0·6916

The asterisk denotes that the values are appropriate to the following reference conditions:

$U_0 = 100$ ft/sec, $a_0 = 1117$ ft/sec, $T_D = T_0$; also $A_t/S' = 4 \times 10^{-4}$ for the values of C_Q^* and C_μ^*.

To scale to other conditions, we write:

$$\frac{v_j}{U_0} = F_v \frac{v_j^*}{U_0}, \quad C_Q = F_Q C_Q^*, \quad C_\mu = F_\mu C_\mu^*$$

where

$$F_v = \frac{100}{U_0} \frac{a_0}{1117} \left(\frac{T_D}{T_0}\right)^{1/2}, \quad F_Q = \frac{100}{U_0} \frac{a_0}{1117} \left(\frac{T_0}{T_D}\right)^{1/2} \frac{(A_t/S')}{4 \times 10^{-4}}$$

$$F_\mu = \frac{100}{U_0} \frac{a_0^2}{(1117)^2} \frac{(A_t/S')}{4 \times 10^{-4}}$$

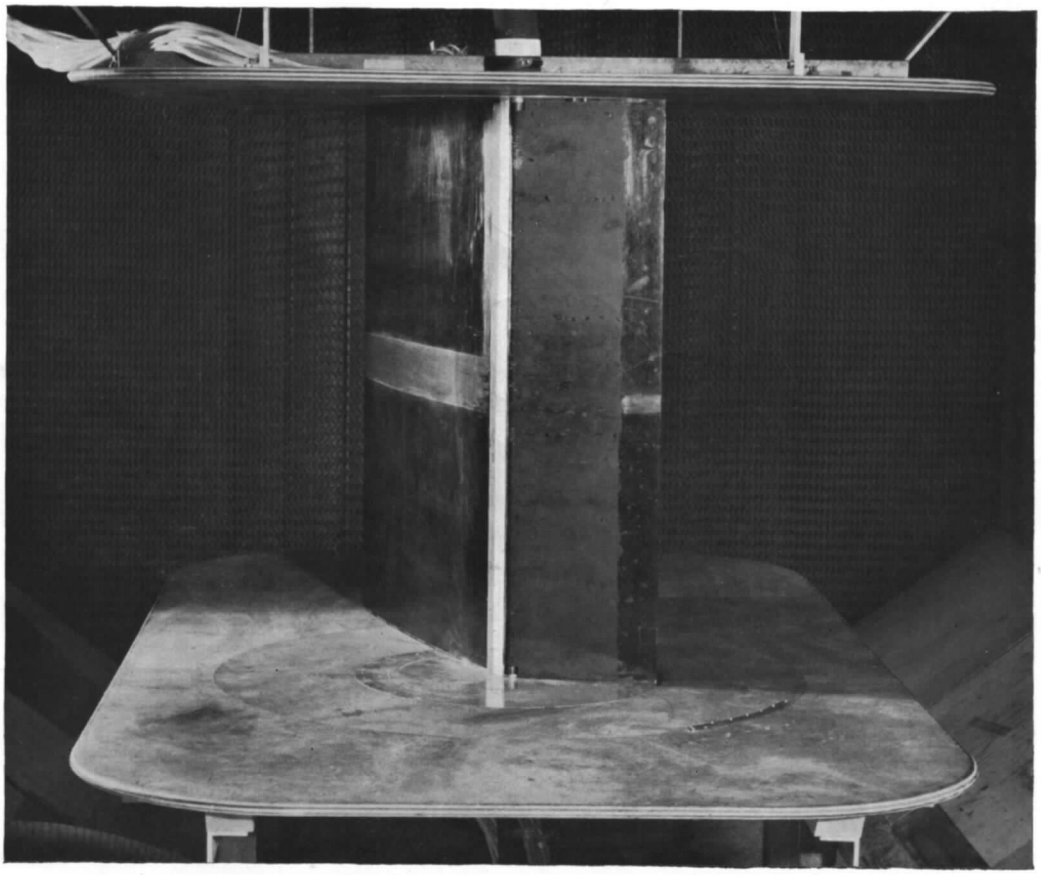

FIG. 1. Trailing-edge flap blowing model.

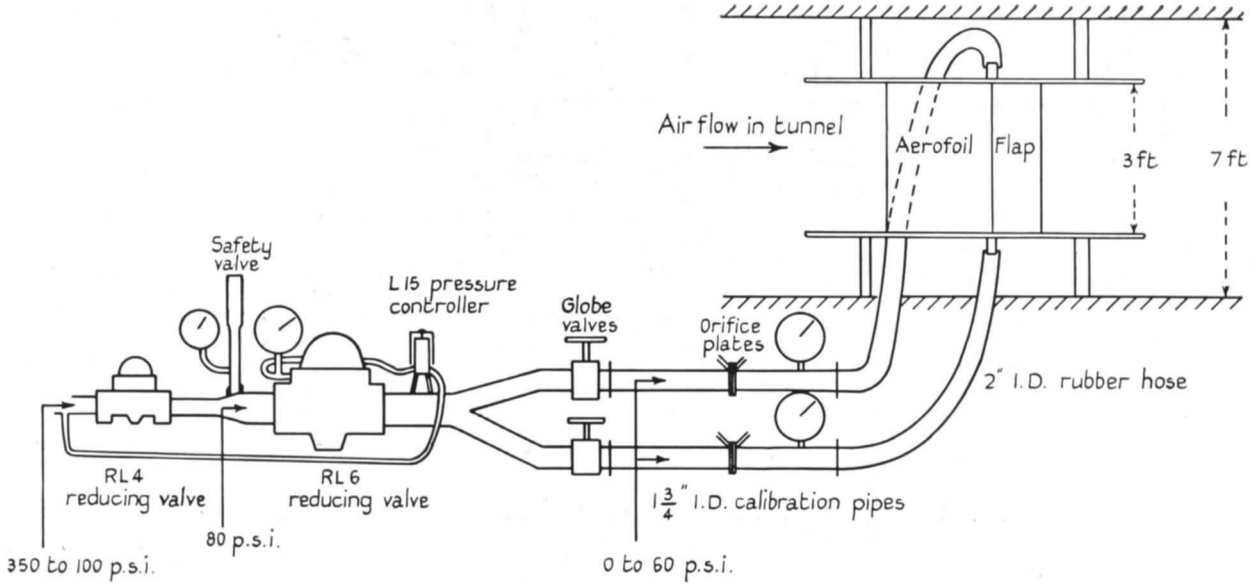

FIG. 2. Arrangement of trailing-edge flap blowing model and external ducting.

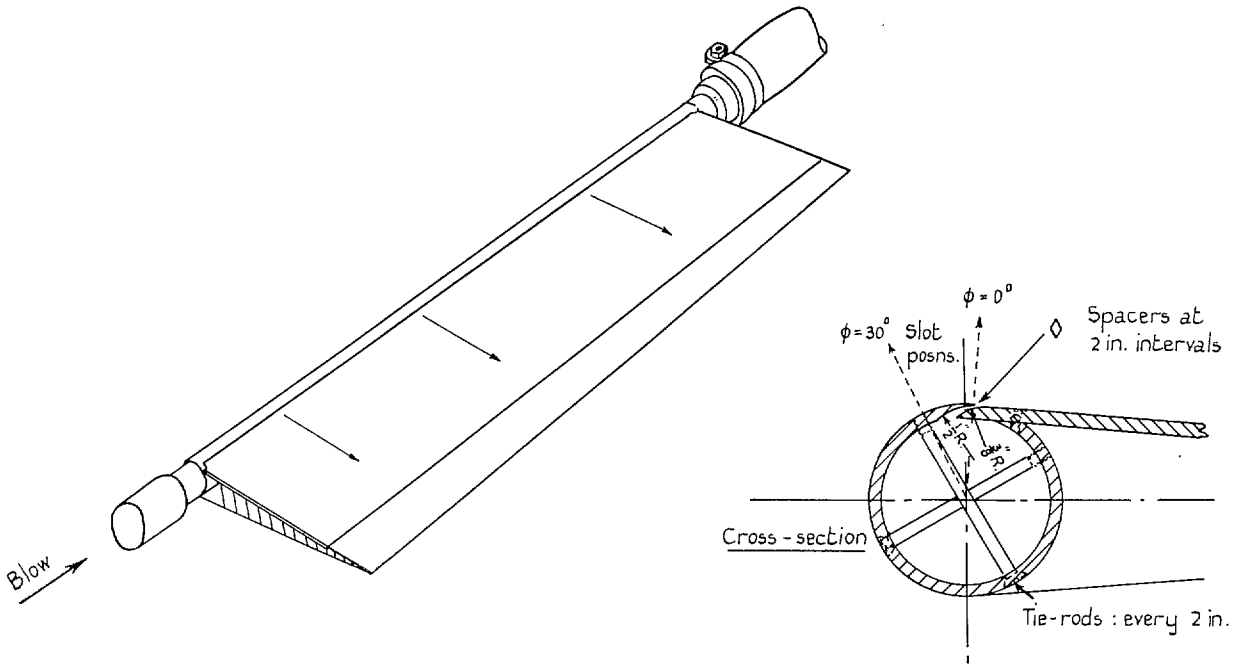

FIG. 3. Blowing duct and slot construction.

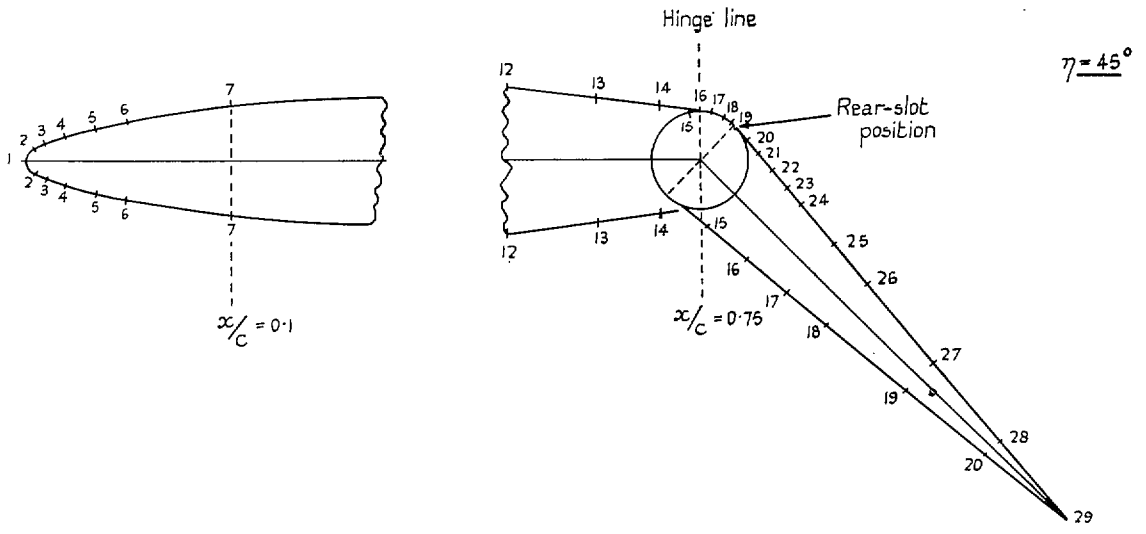

FIG. 4. Static-pressure hole positions on wing nose and trailing-edge flap.

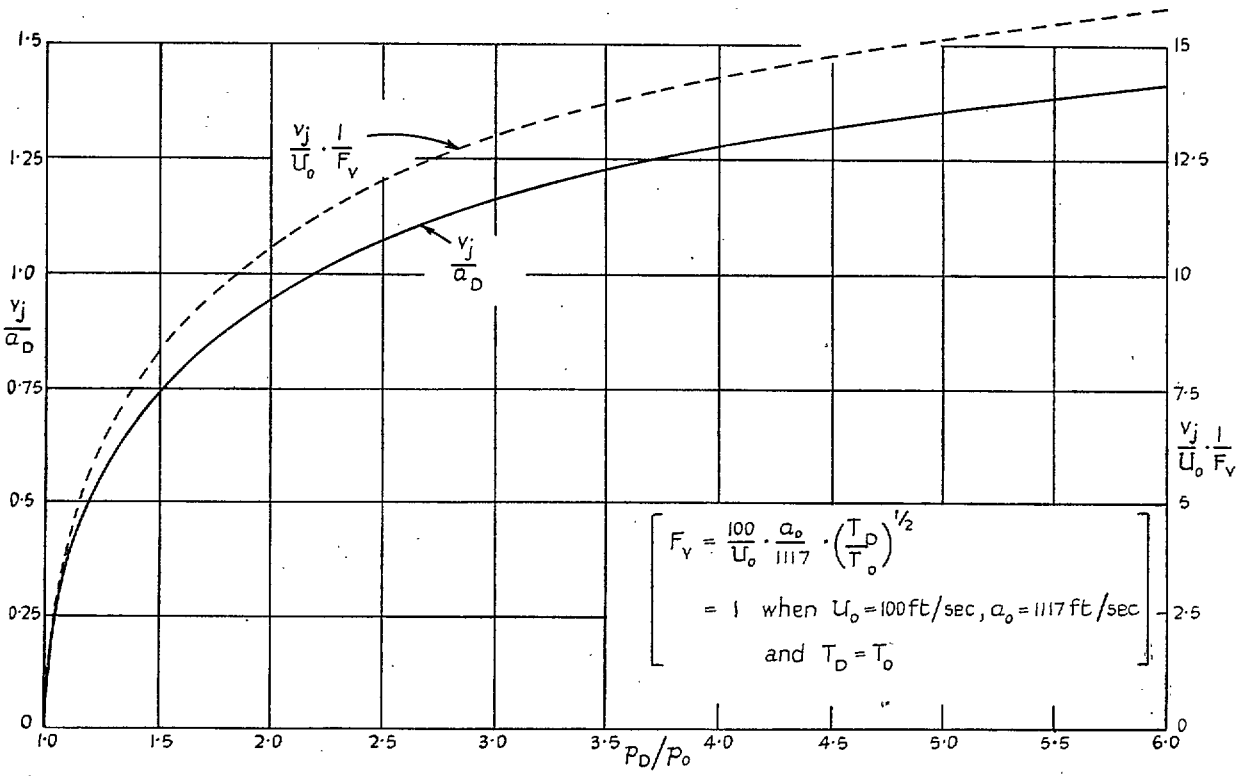

FIG. 5. Theoretical variation of blowing velocity with blowing pressure ratio.

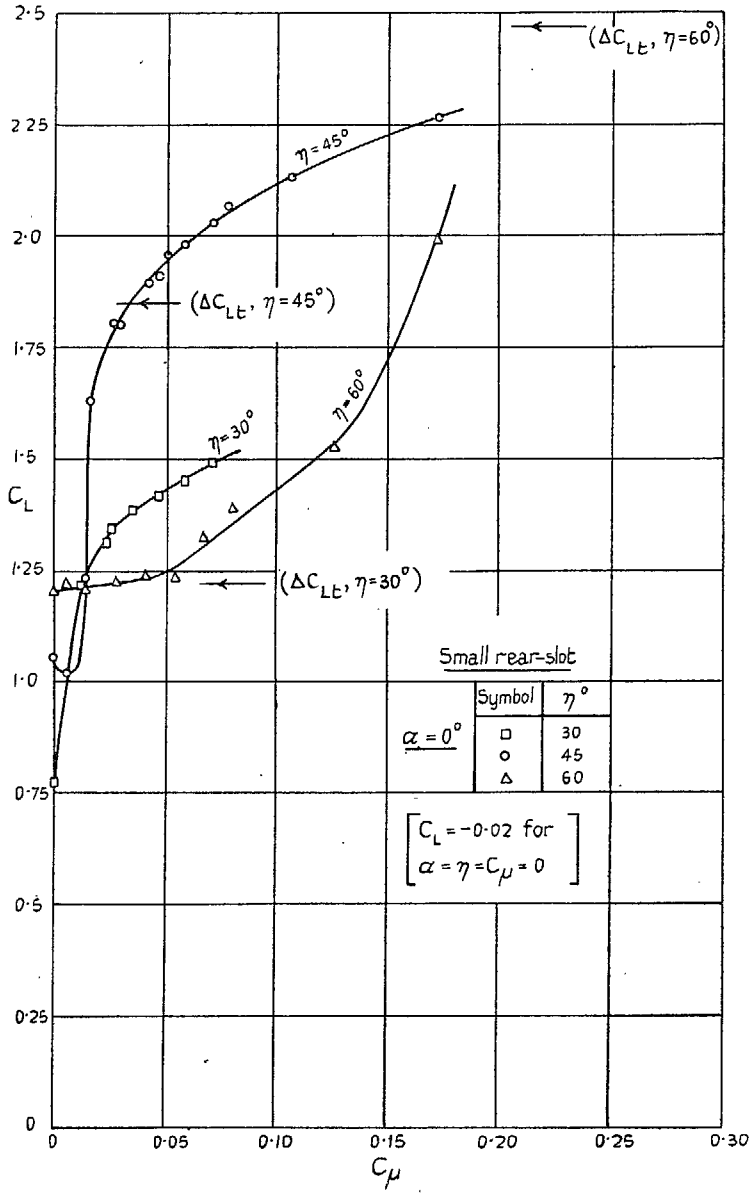

FIG. 6a. Variation of flap lift increment with momentum coefficient and flap angle at 0 deg incidence.

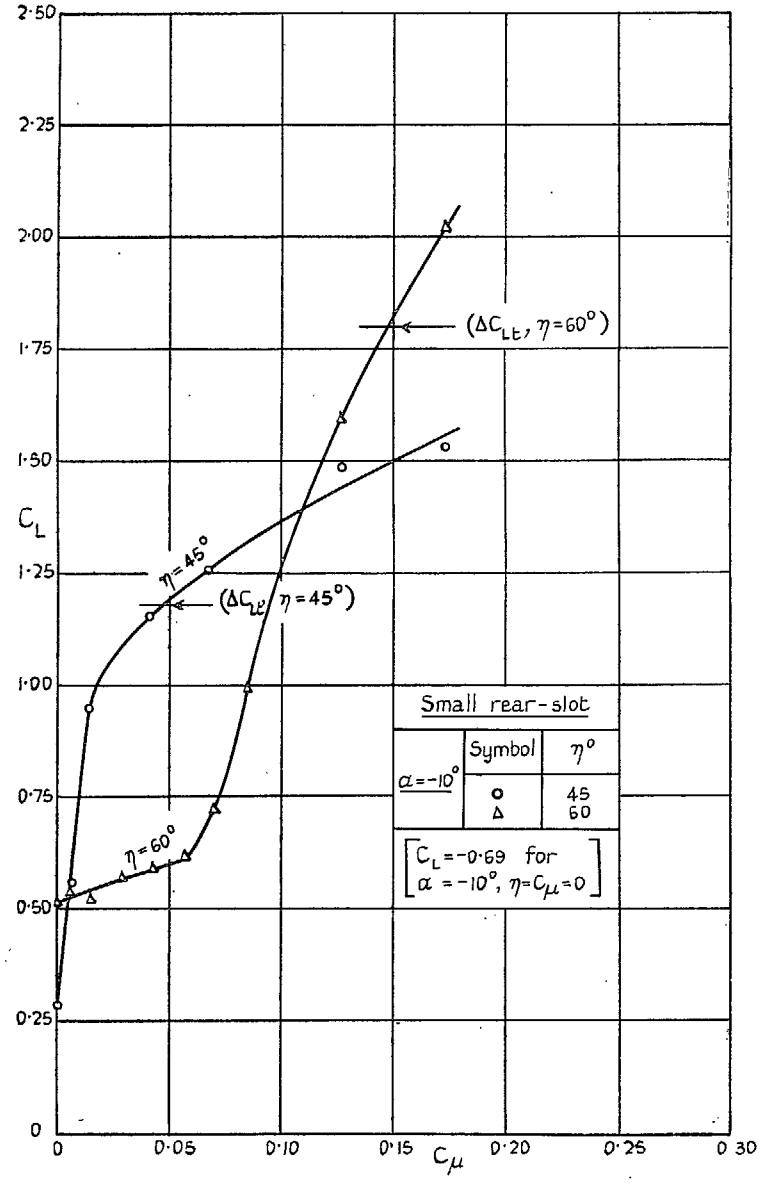

FIG. 6b. Variation of flap lift increment with momentum coefficient and flap angle at — 10 deg incidence.

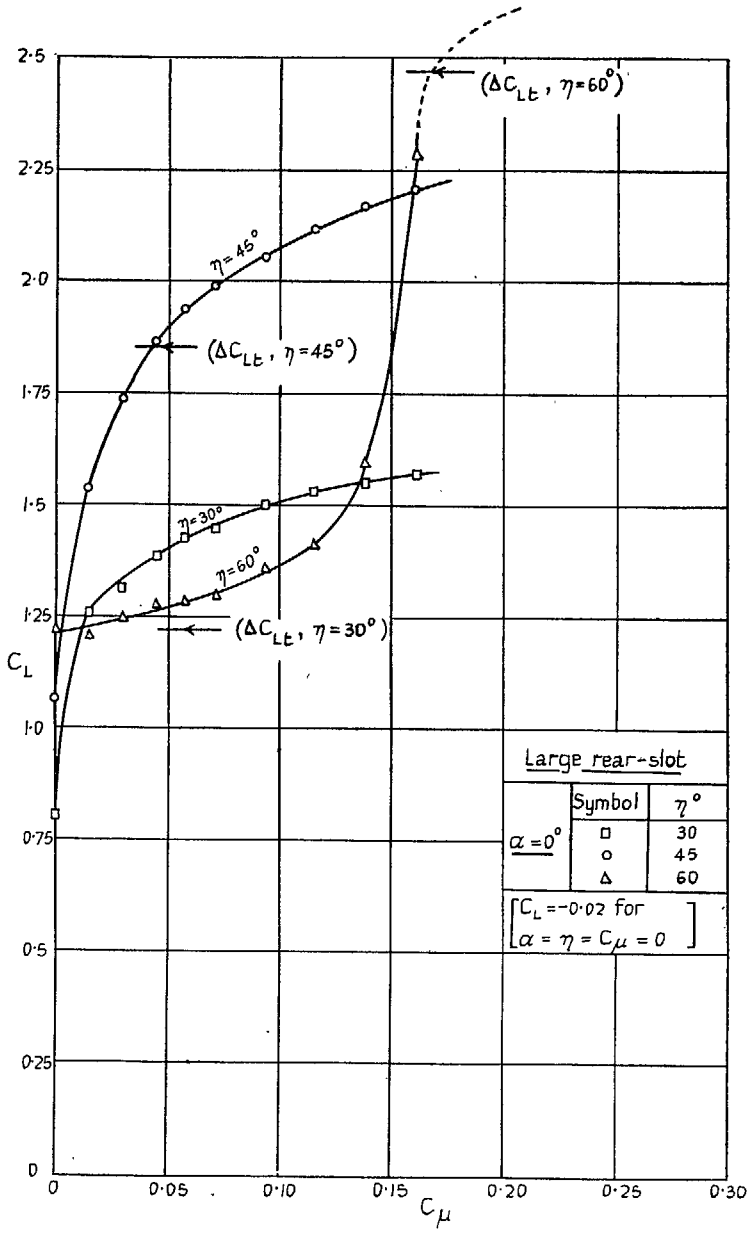

FIG. 7a. Variation of flap lift increment with momentum coefficient and flap angle at 0 deg incidence.

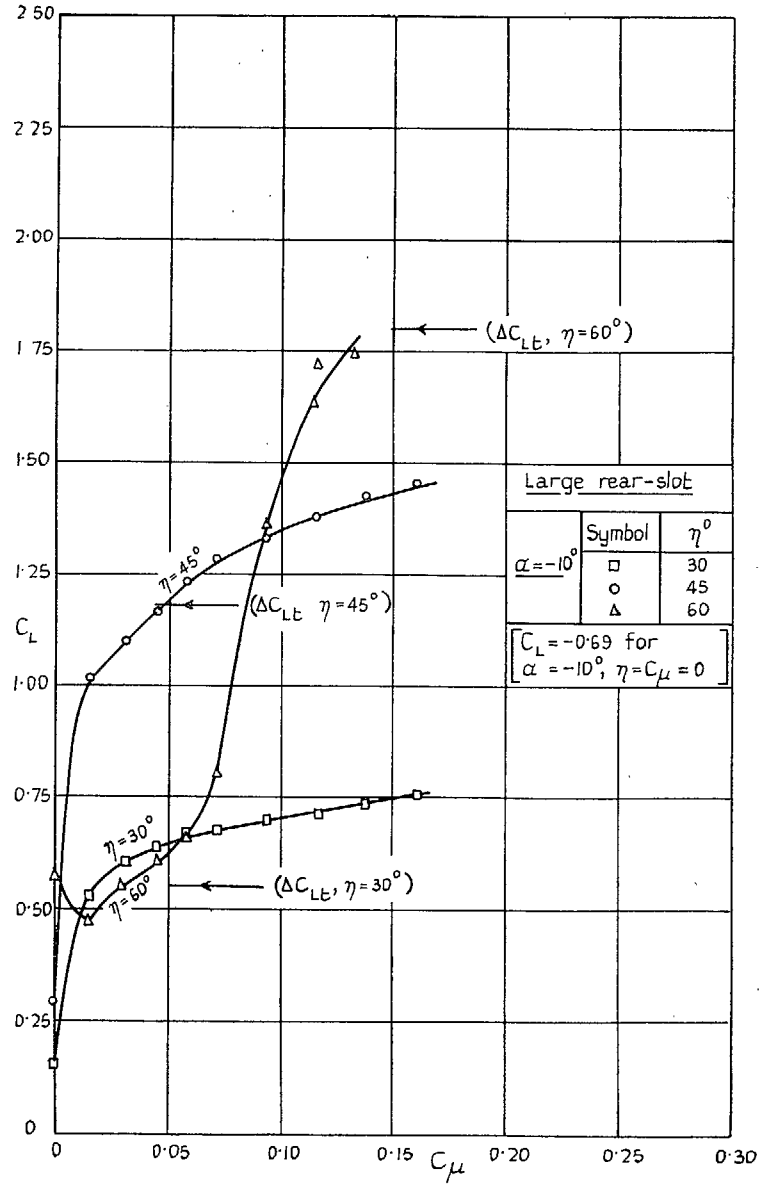

FIG. 7b. Variation of flap lift increment with momentum coefficient and flap angle at — 10 deg incidence.

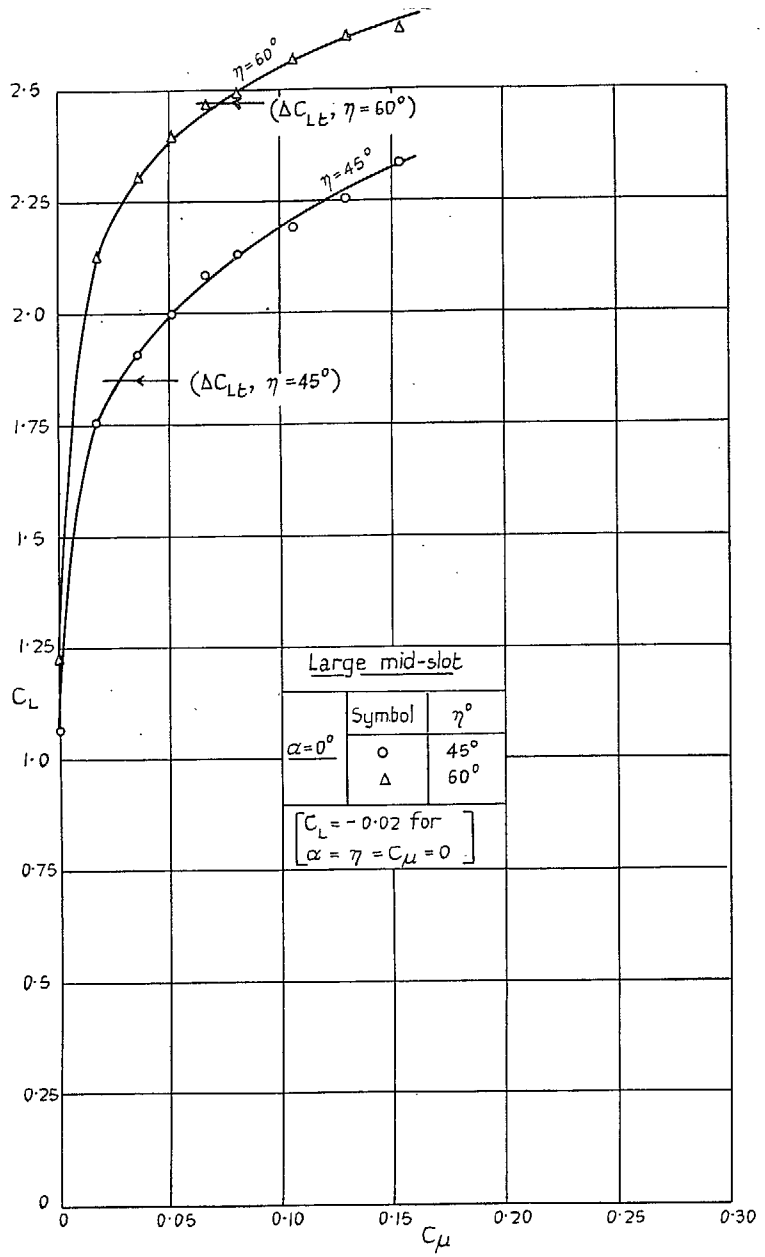

FIG. 8a. Variation of flap lift increment with momentum coefficient and flap angle at 0 deg incidence.

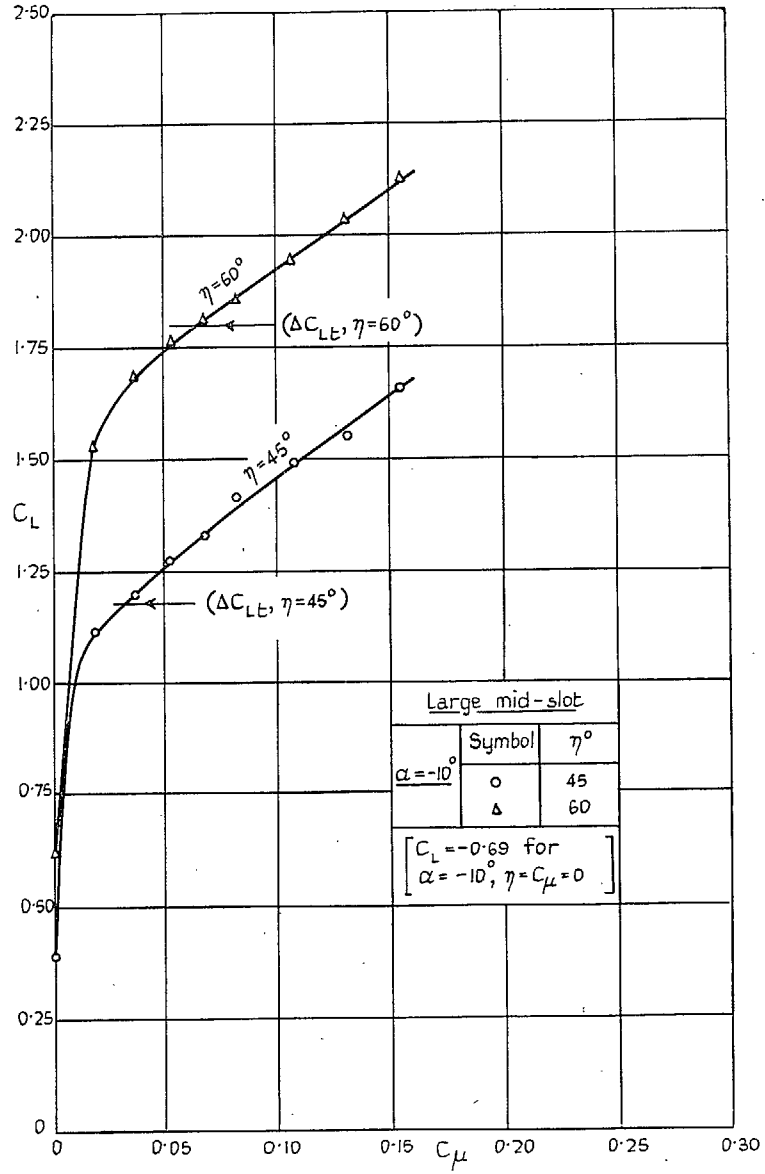

FIG. 8b. Variation of flap lift increment with momentum coefficient and flap angle at — 10 deg incidence.

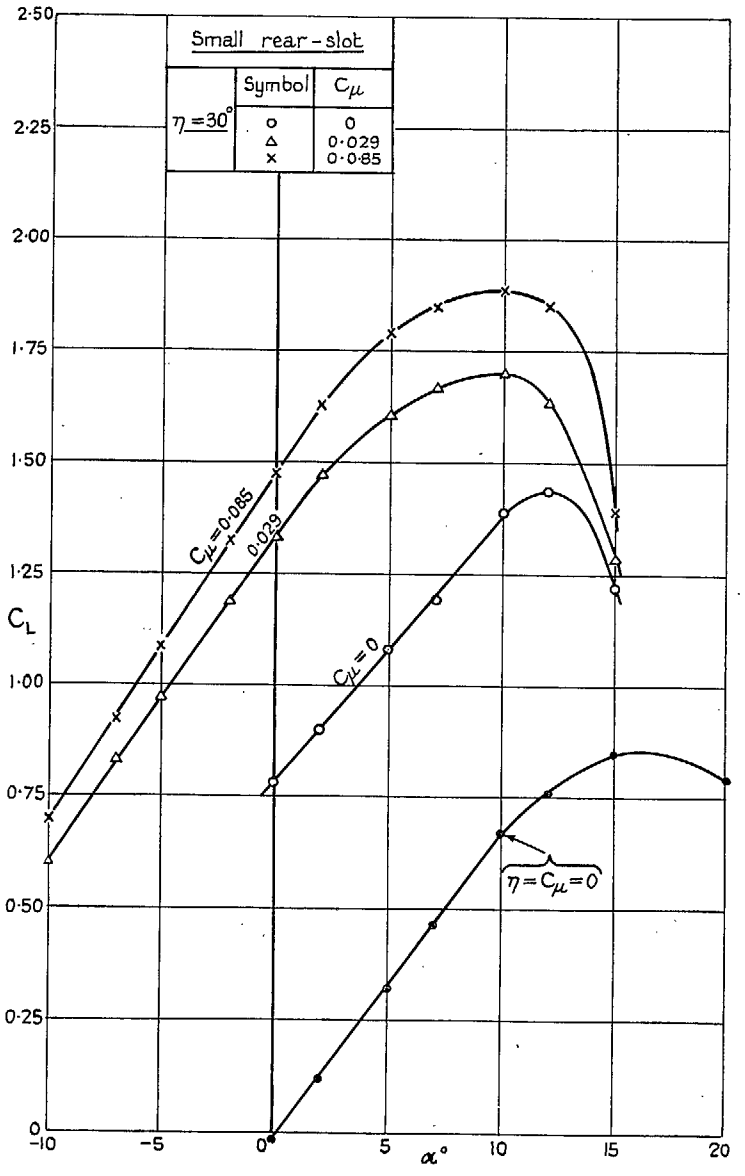

FIG. 9a. Variation of lift with incidence at constant C_μ for $\eta = 30$ deg.

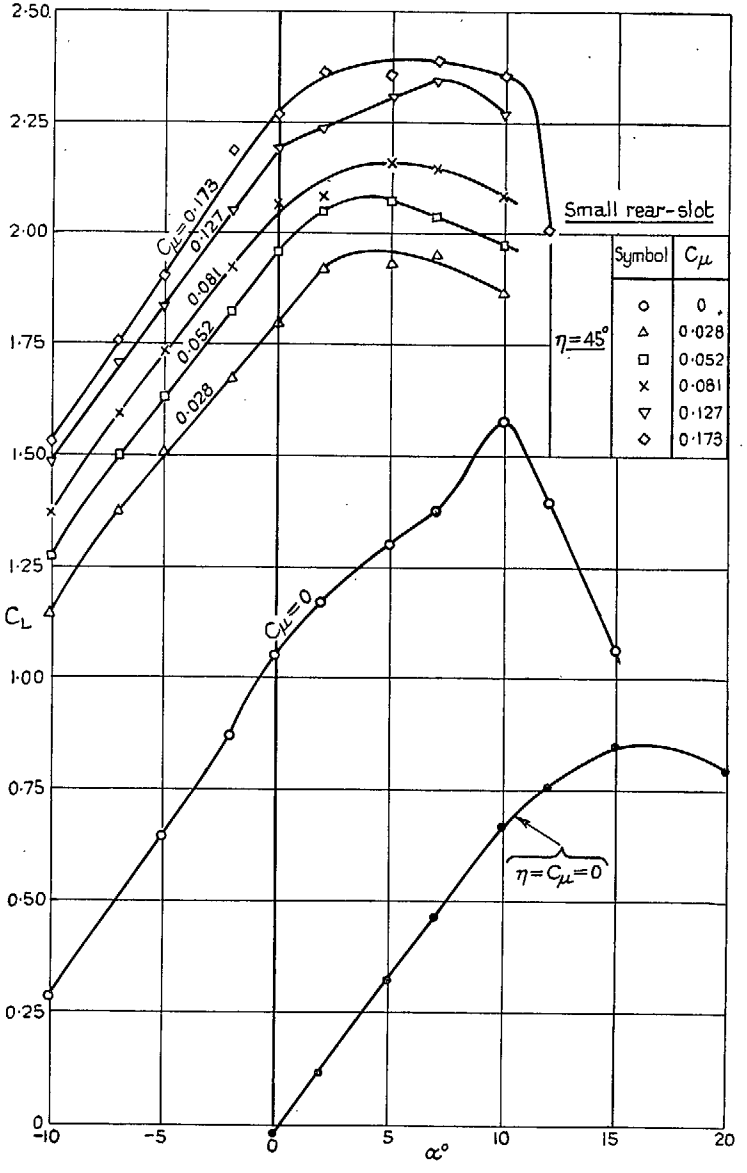

FIG. 9b. Variation of lift with incidence at constant C_μ for $\eta = 45$ deg.

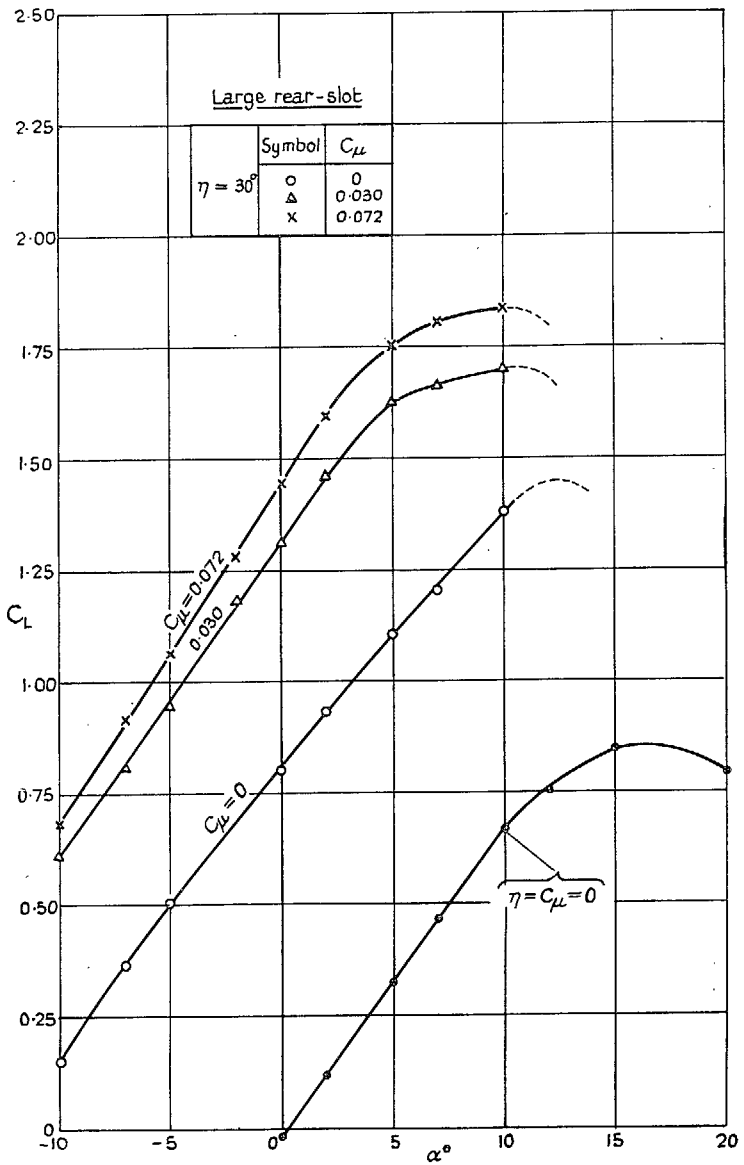

FIG. 10a. Variation of lift with incidence at constant C_μ for $\eta = 30$ deg.

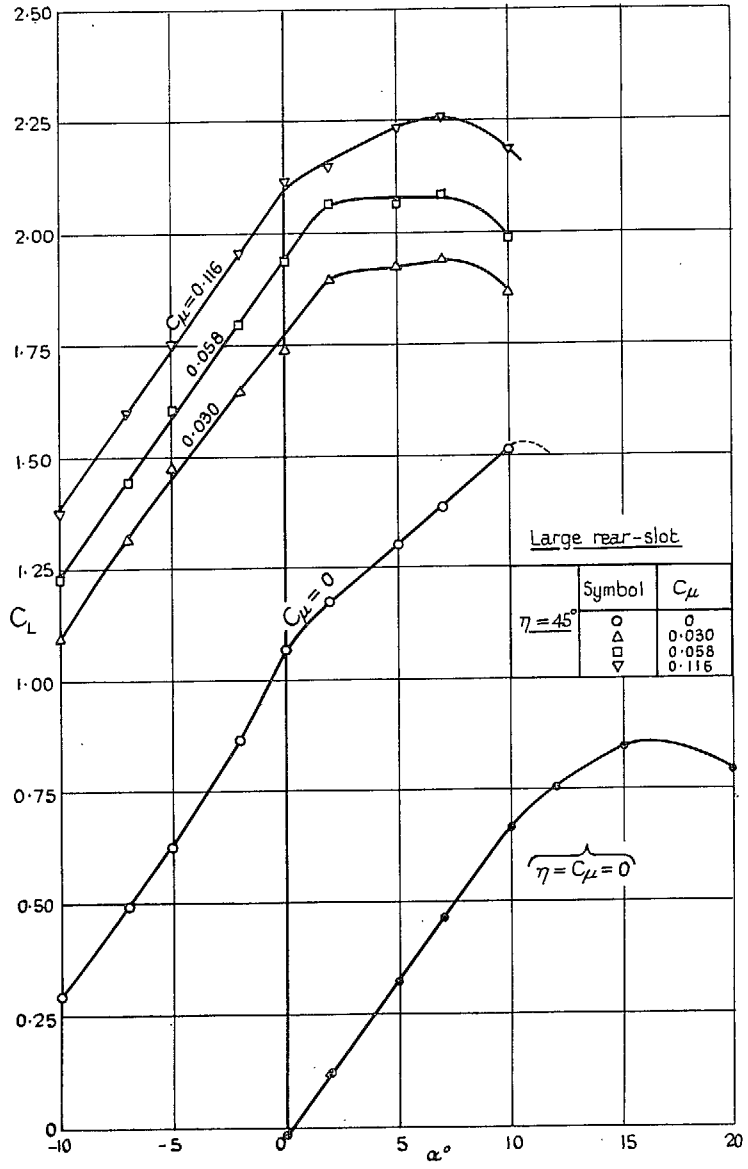

FIG. 10b. Variation of lift with incidence at constant C_μ for $\eta = 45$ deg.

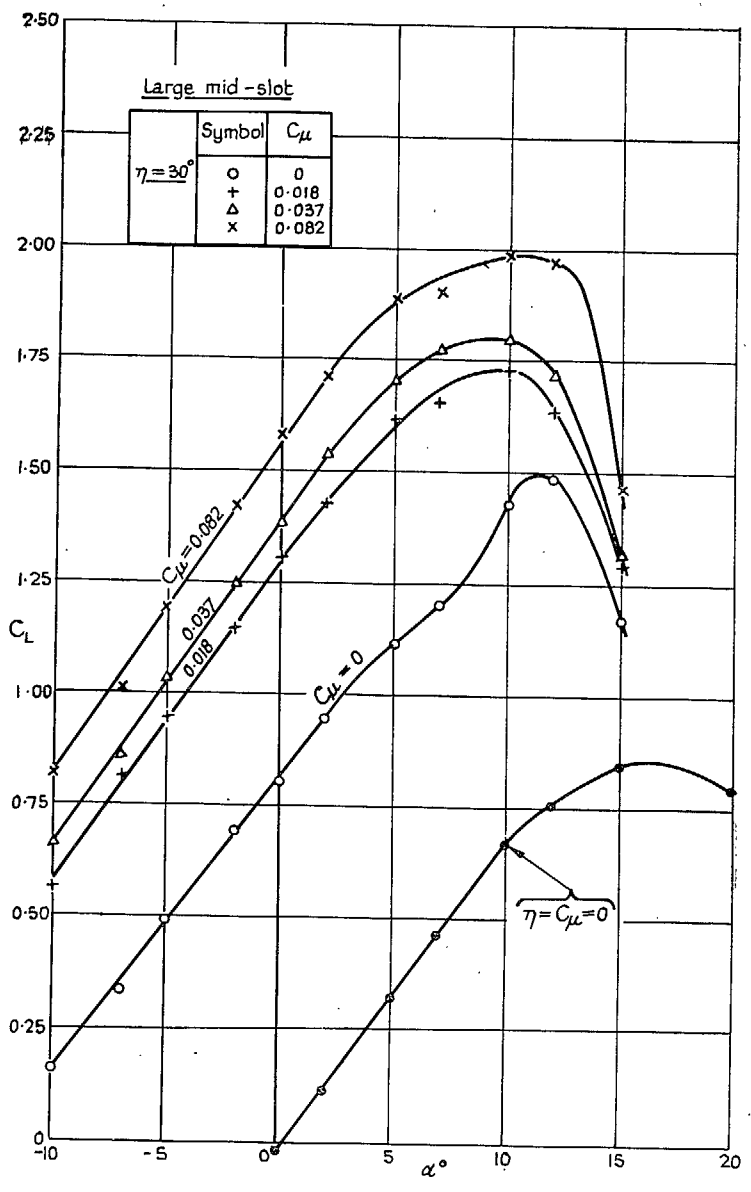

FIG. 11a. Variation of lift with incidence at constant C_μ for $\eta = 30$ deg.

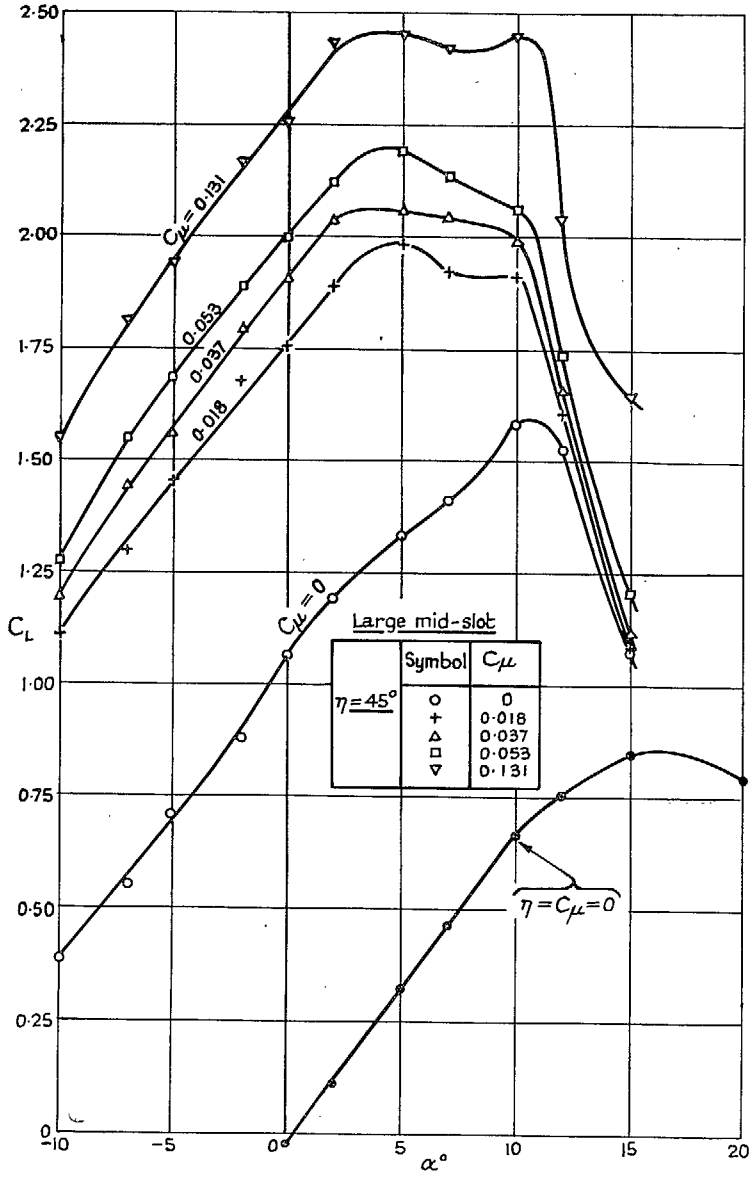

FIG. 11b. Variation of lift with incidence at constant C_μ for $\eta = 45$ deg.

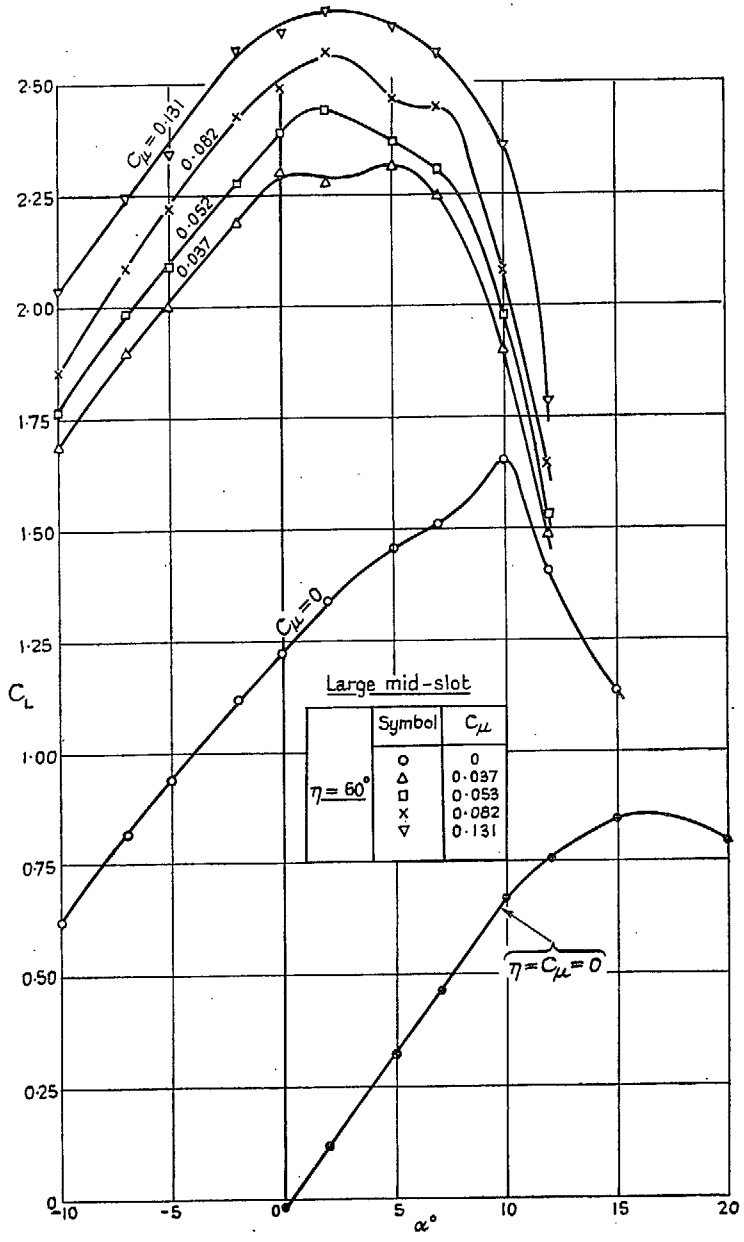

FIG. 11c. Variation of lift with incidence at constant C_μ for $\eta = 60$ deg.

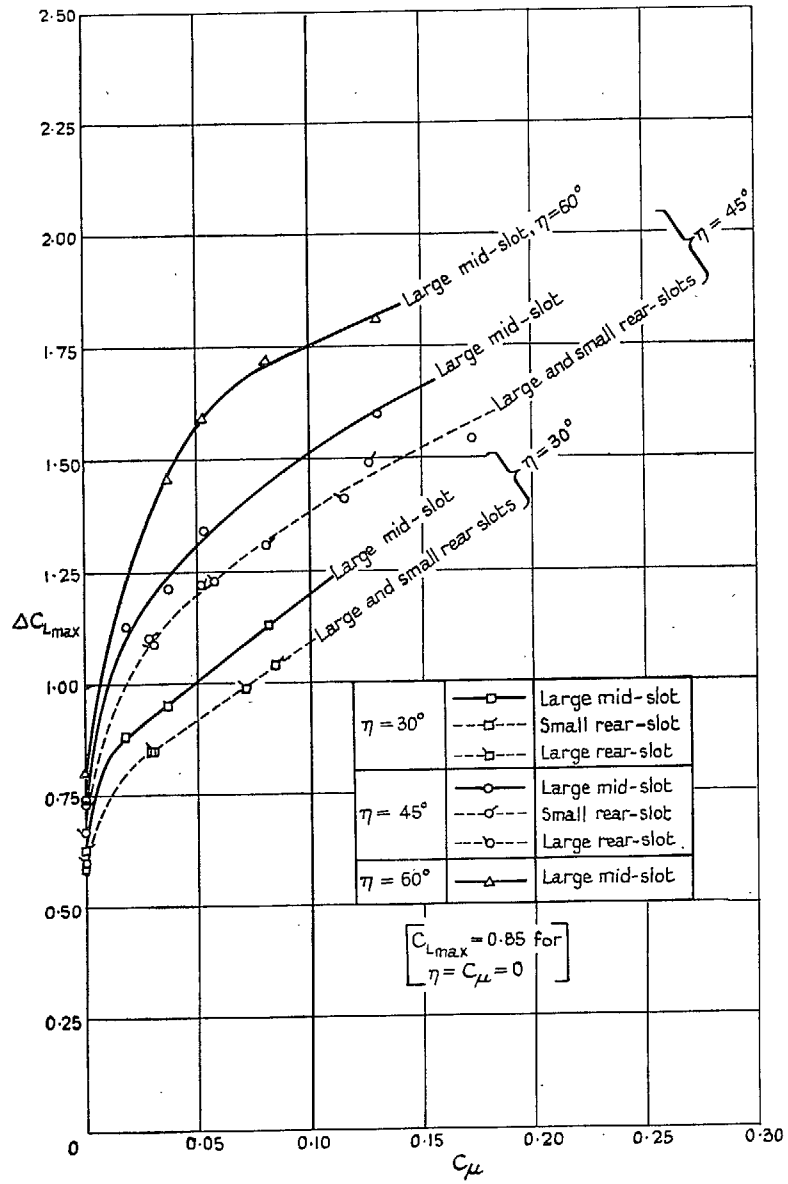

FIG. 12. Variation of $\Delta C_{L\max}$ with C_μ at constant flap angle.

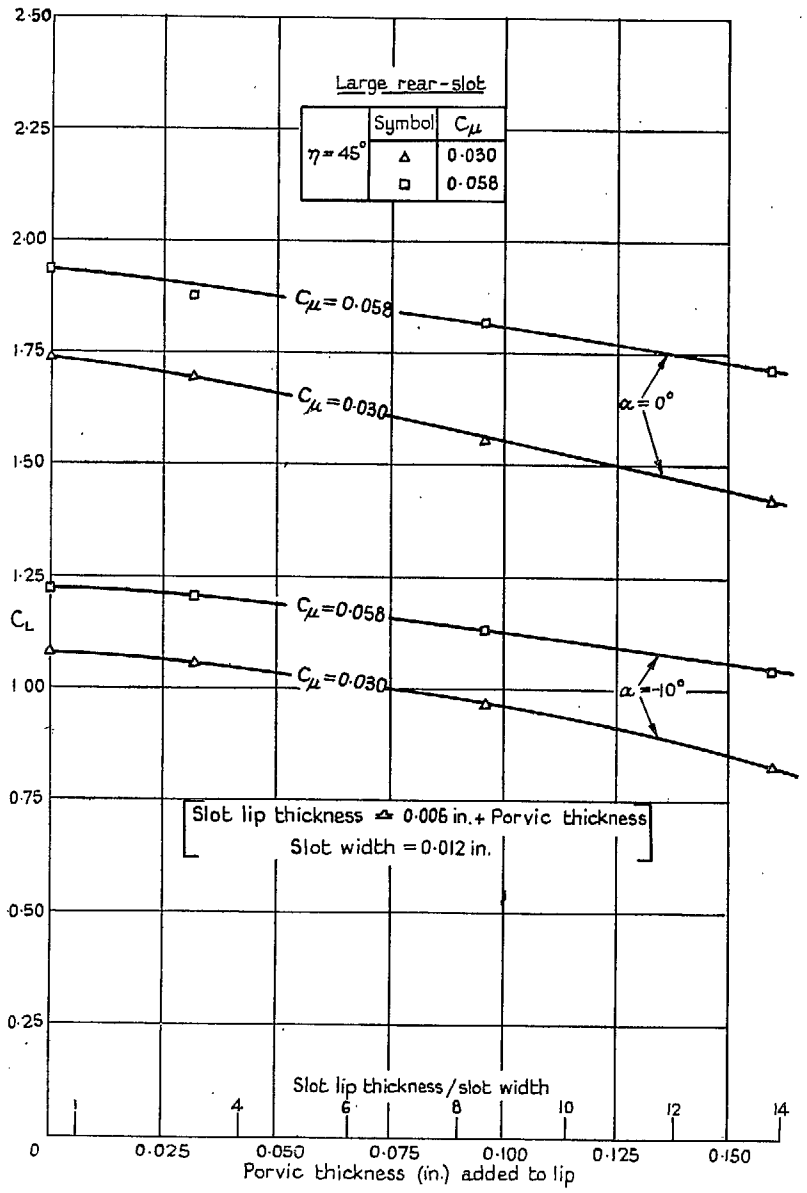

FIG. 13. Variation of C_L with increase in slot lip thickness.

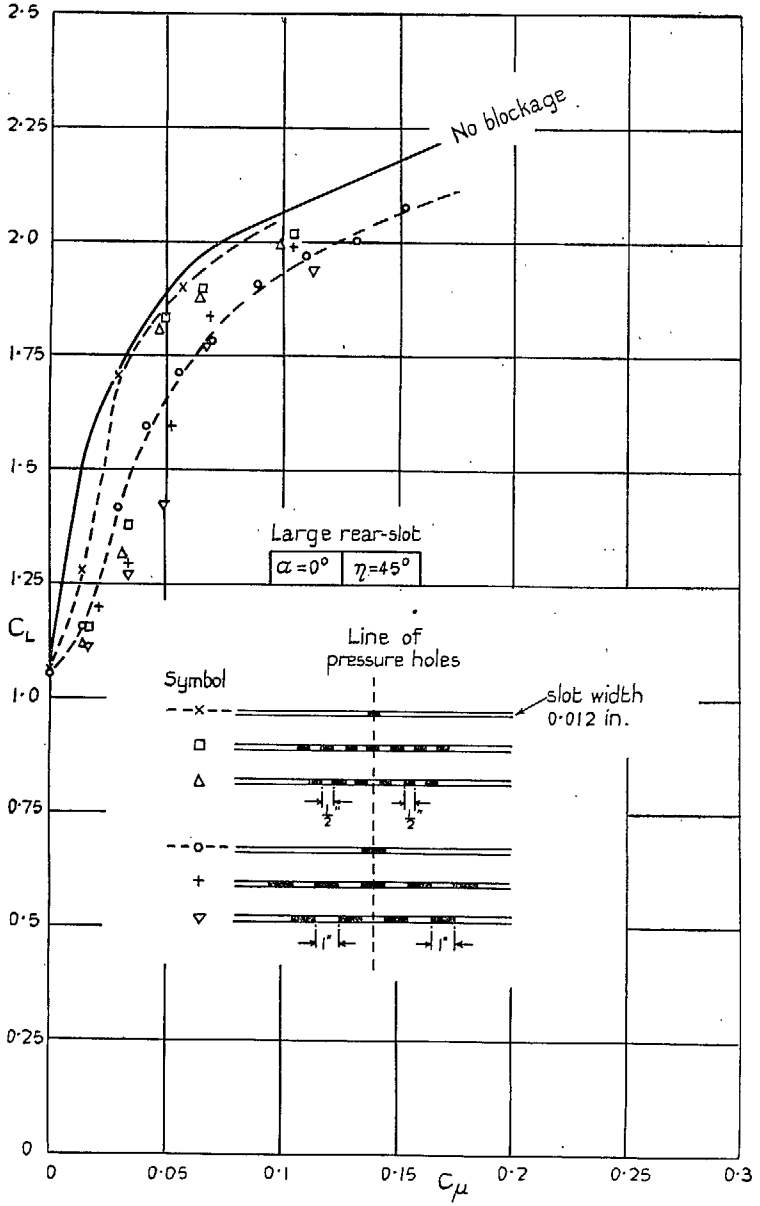

FIG. 14. Variation of lift with slot blockage.

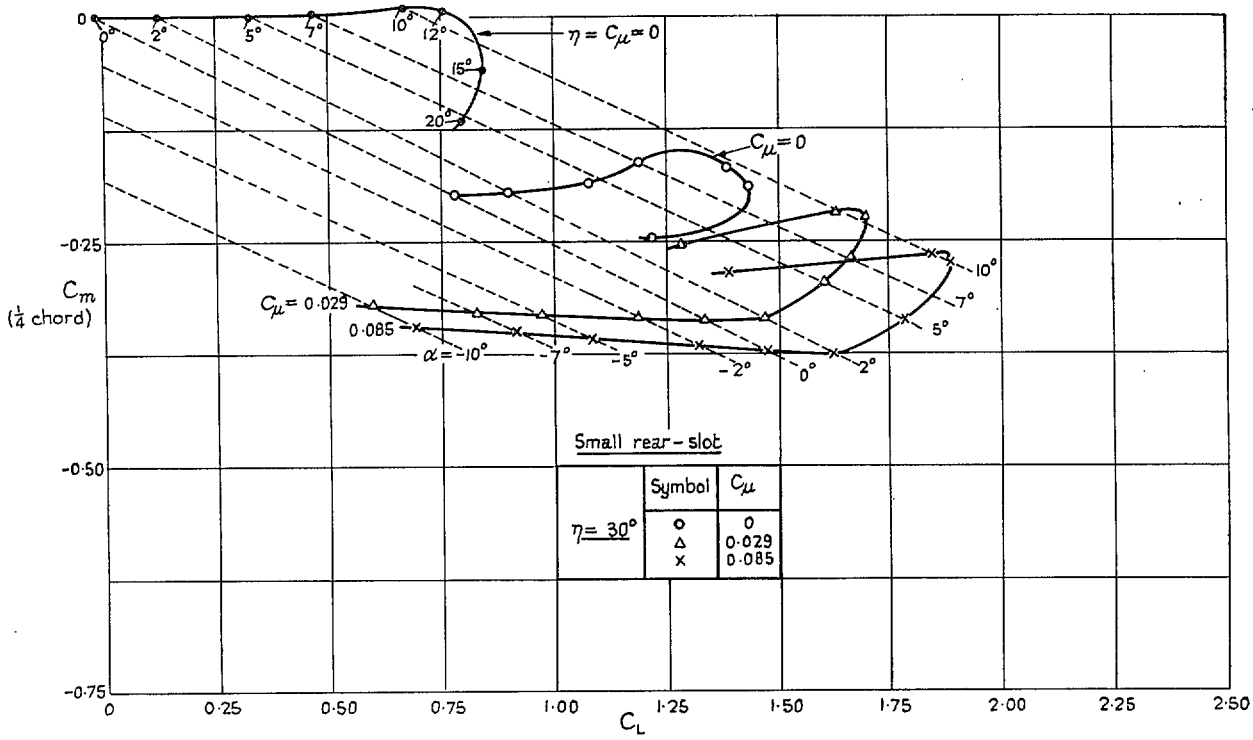

FIG. 15a. Variation of pitching moment with lift at constant C_μ for $\eta = 30$ deg.

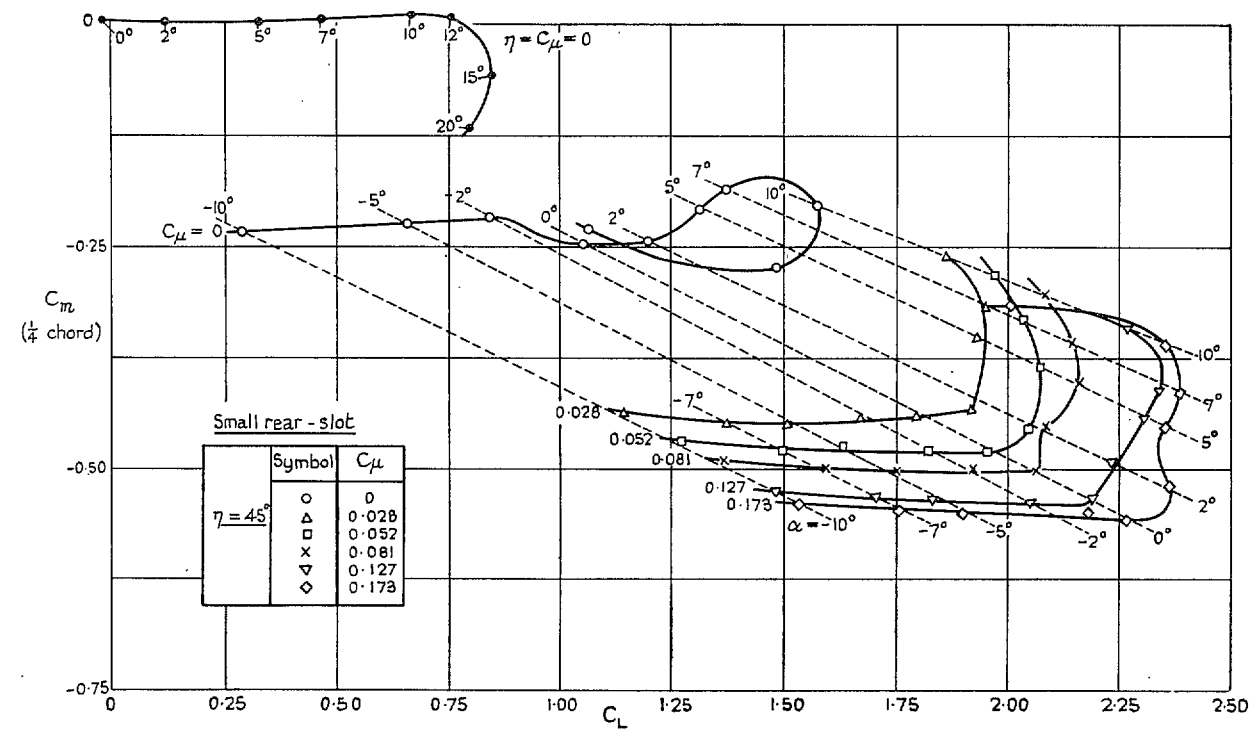

FIG. 15b. Variation of pitching moment with lift at constant C_μ for $\eta = 45$ deg.

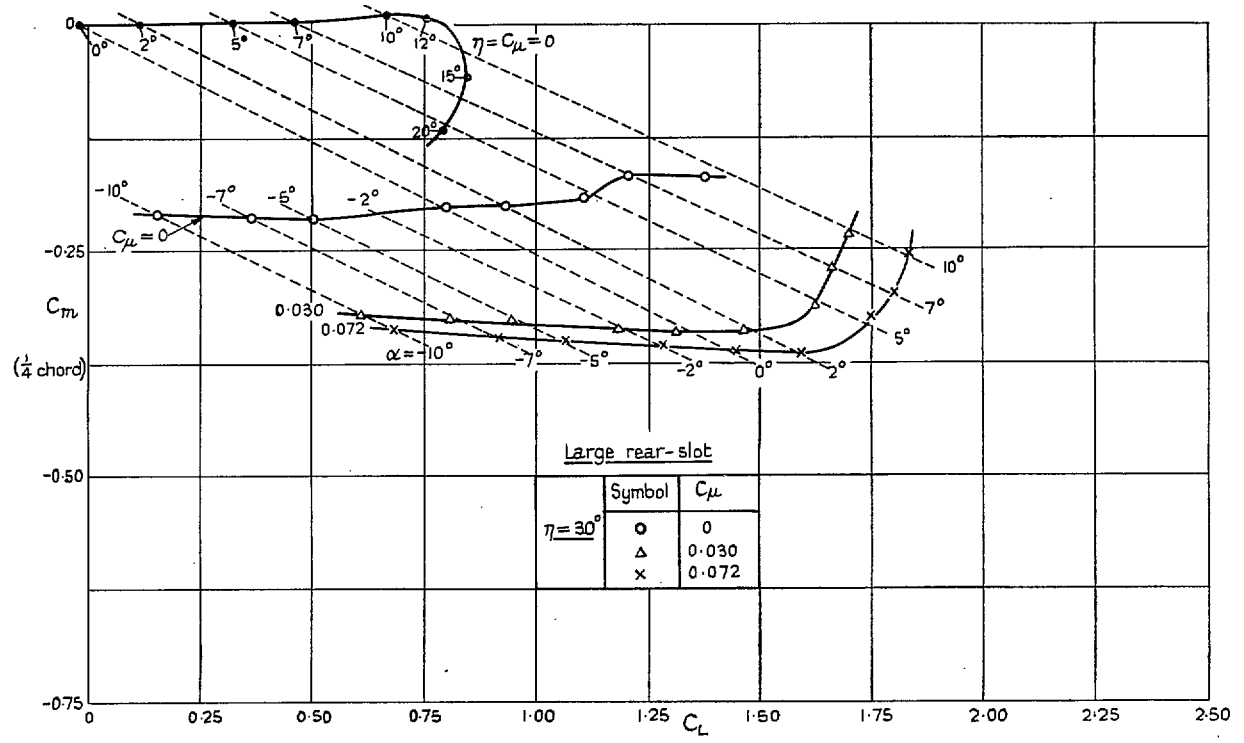

FIG. 16a. Variation of pitching moment with lift at constant C_μ for $\eta = 30$ deg.

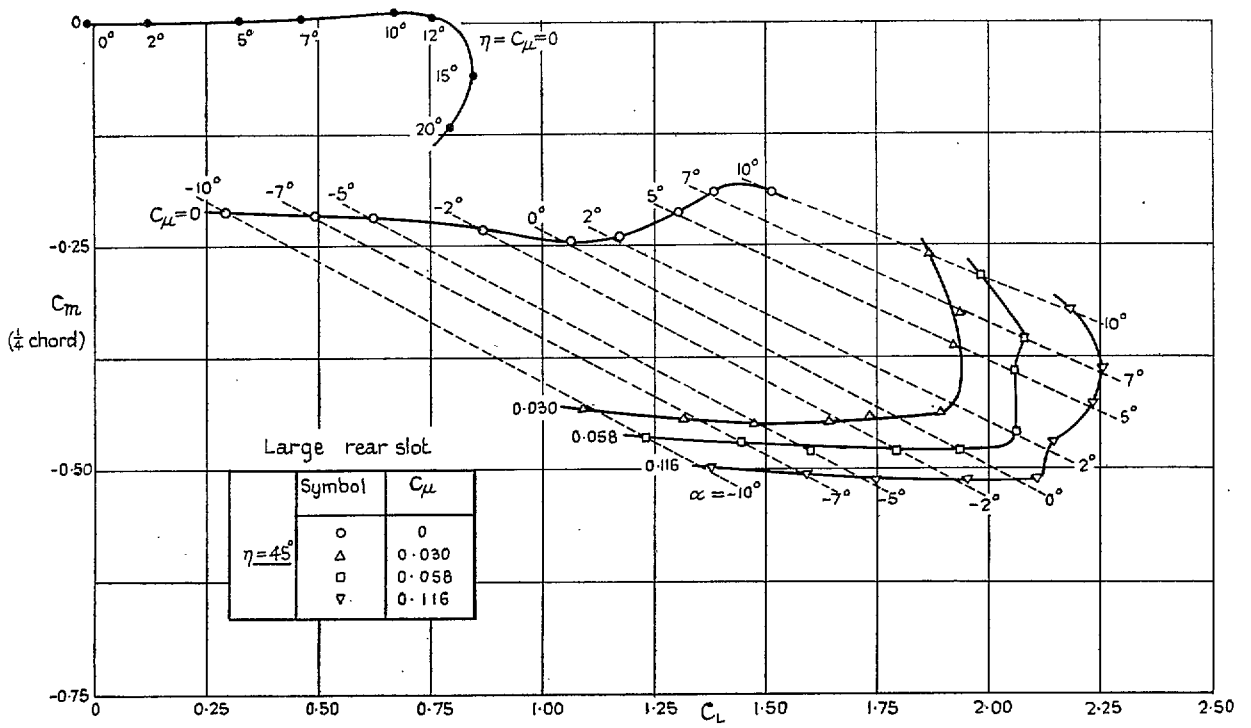

FIG 16b. Variation of pitching moment with lift at constant C_μ for $\eta = 45$ deg.

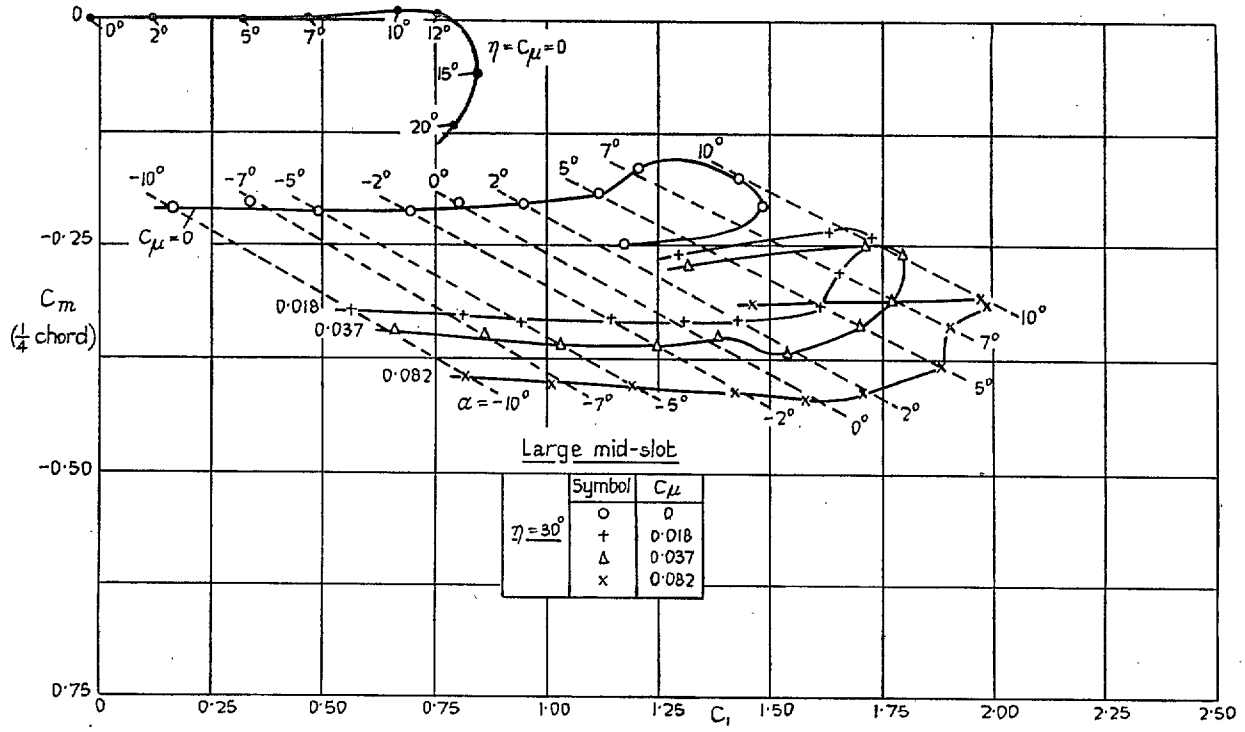

FIG. 17a. Variation of pitching moment with lift at constant C_μ for $\eta = 30$ deg.

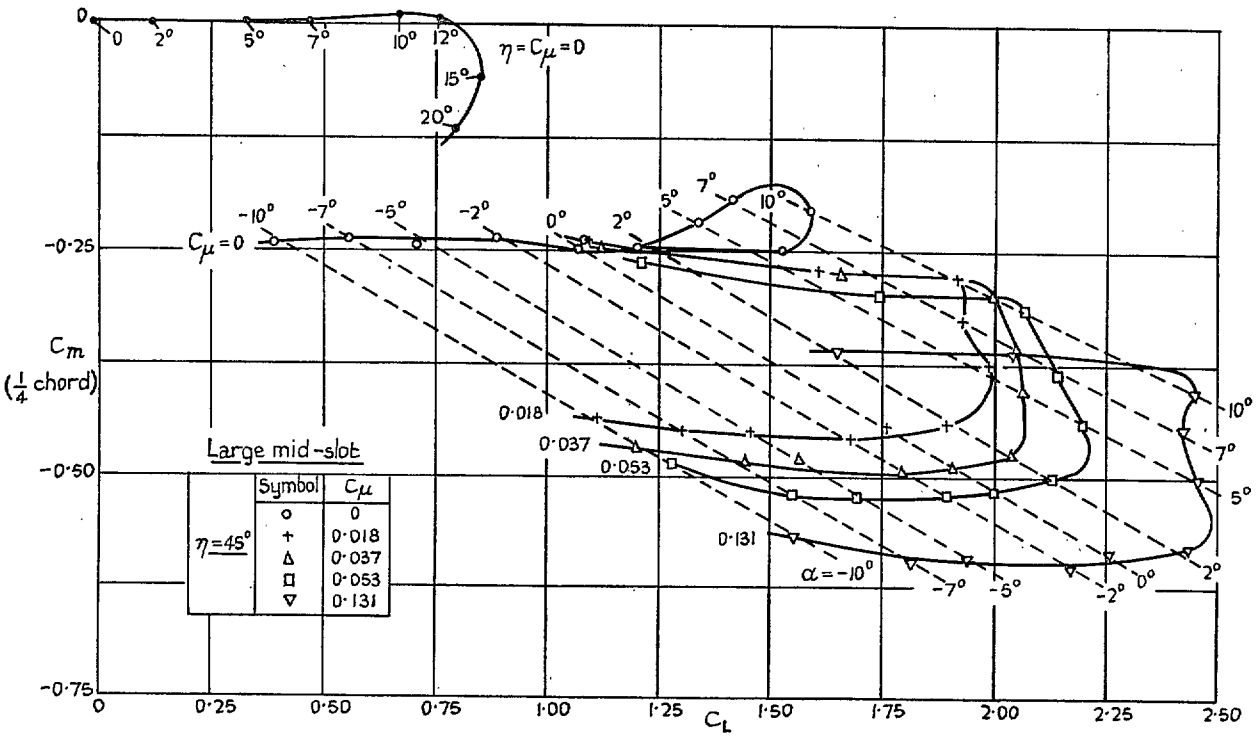

FIG. 17b. Variation of pitching moment with lift at constant C_μ for $\eta = 45$ deg.

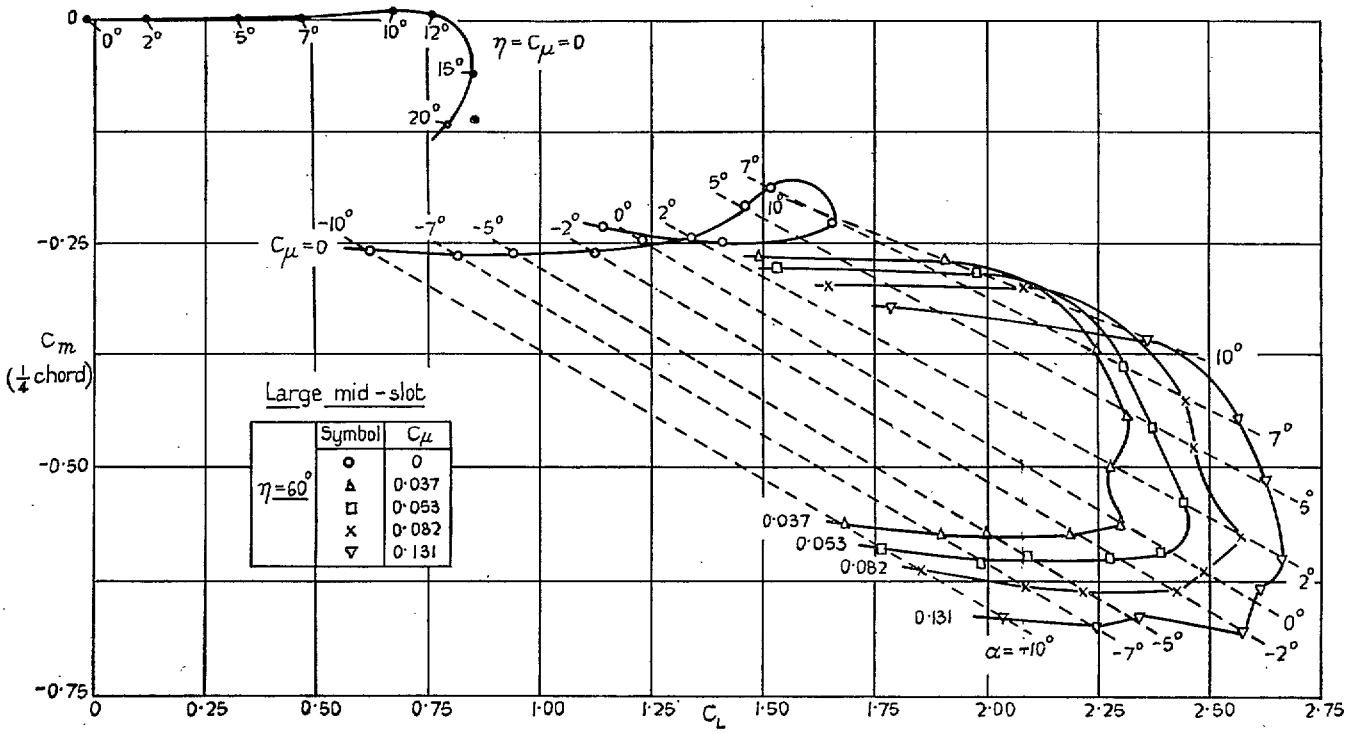

FIG. 17c. Variation of pitching moment with lift at constant C_μ for $\eta = 60$ deg.

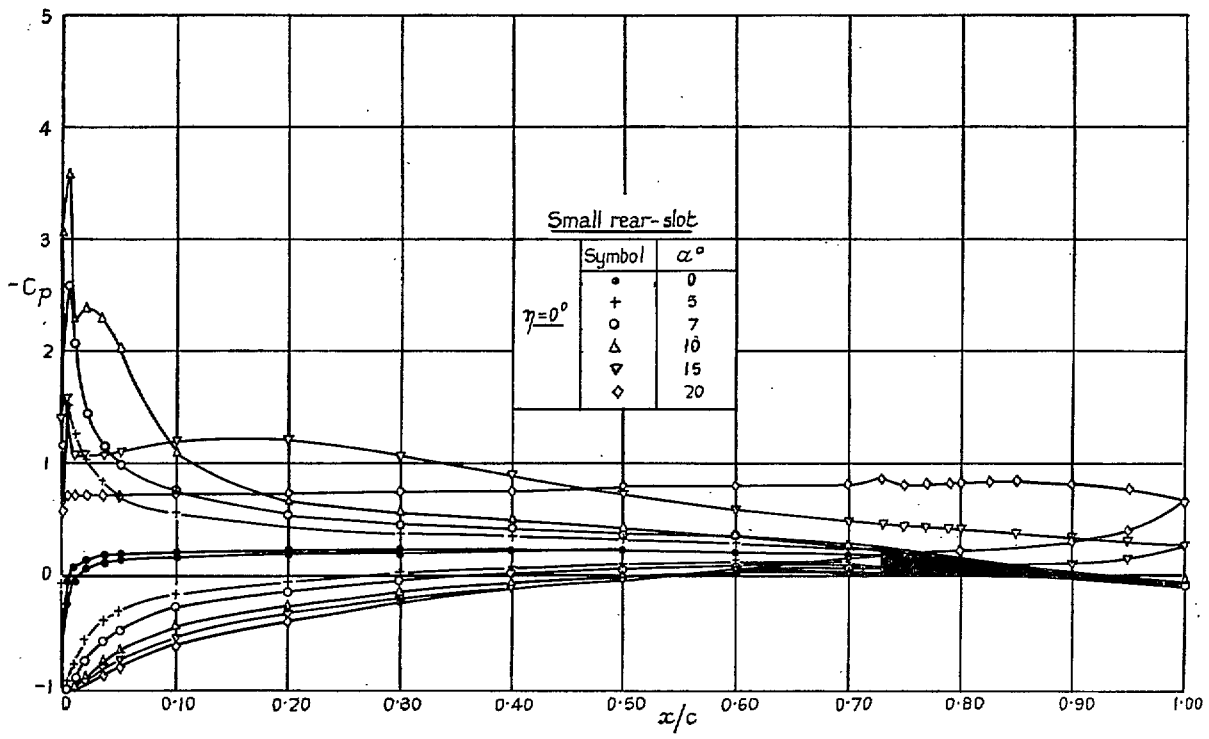

FIG. 18. Variation of pressure distribution with incidence for plain aerofoil.

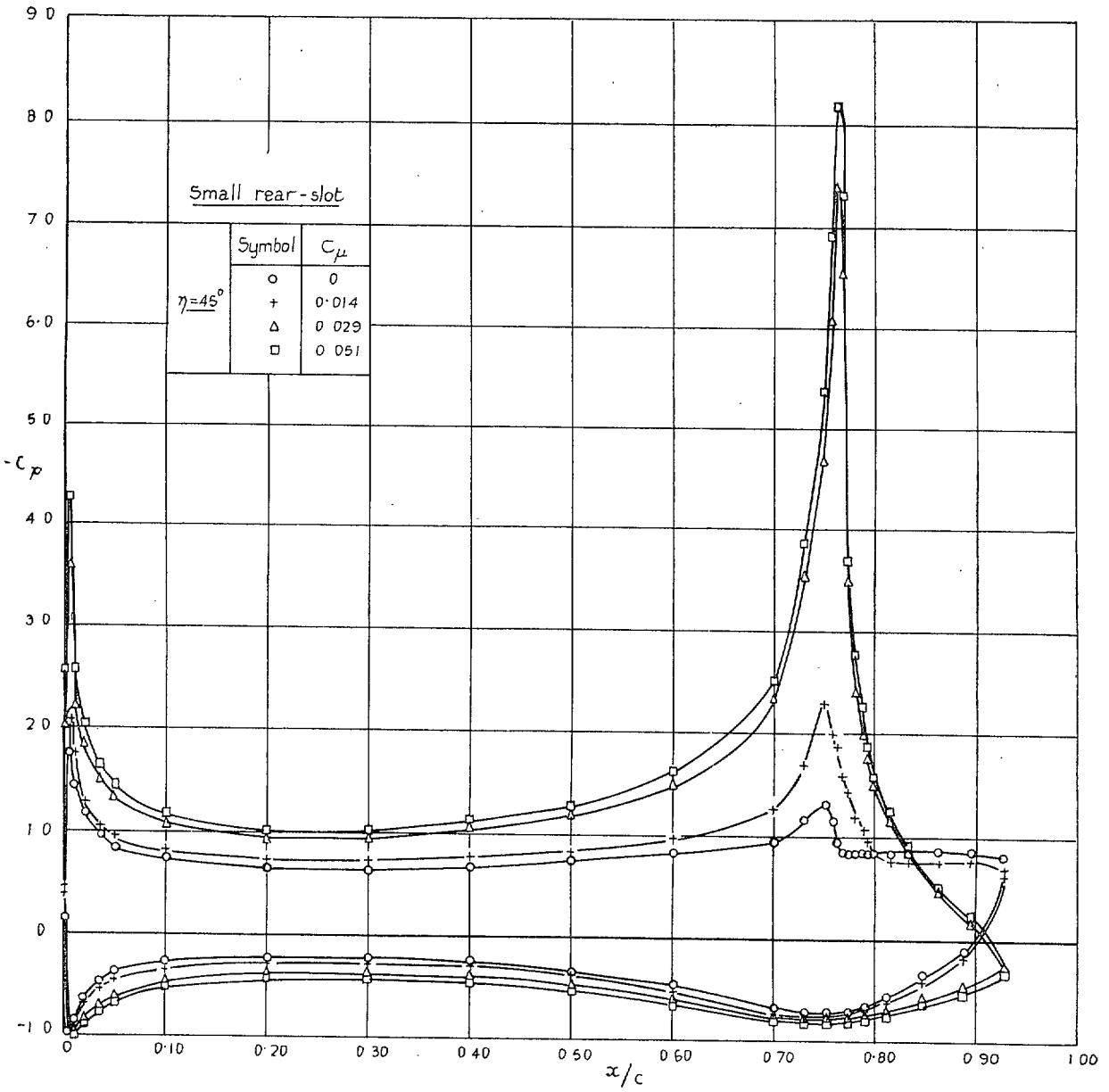

FIG. 19a. Variation of pressure distribution with C_μ for $\eta = 45$ deg and small rear slot.

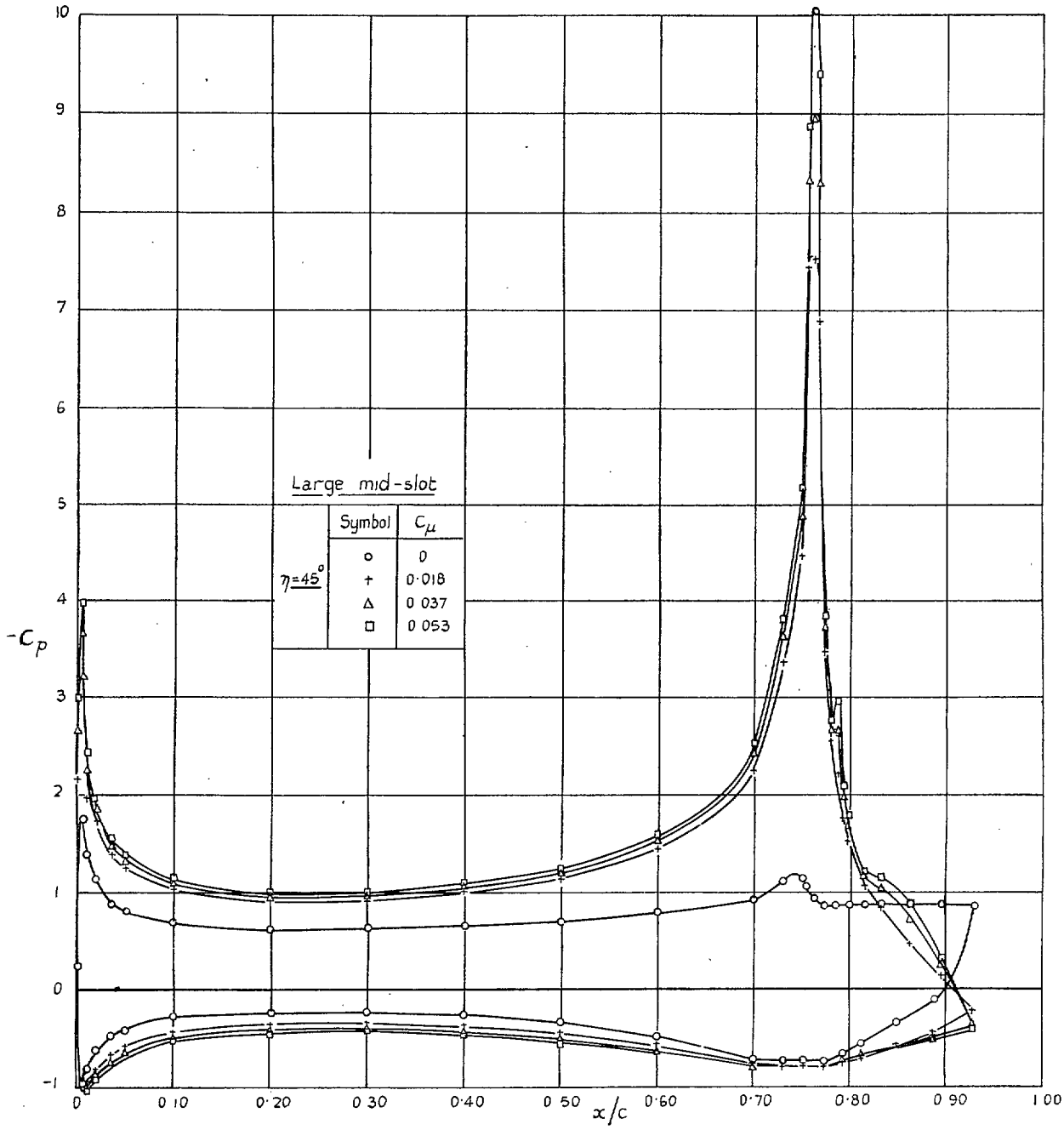

FIG. 19b. Variation of pressure distribution with C_μ for $\eta = 45$ deg and large mid-slot.

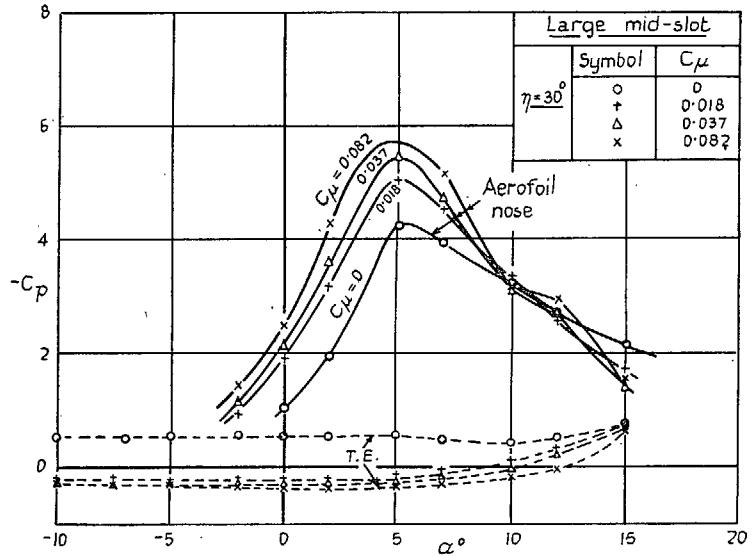

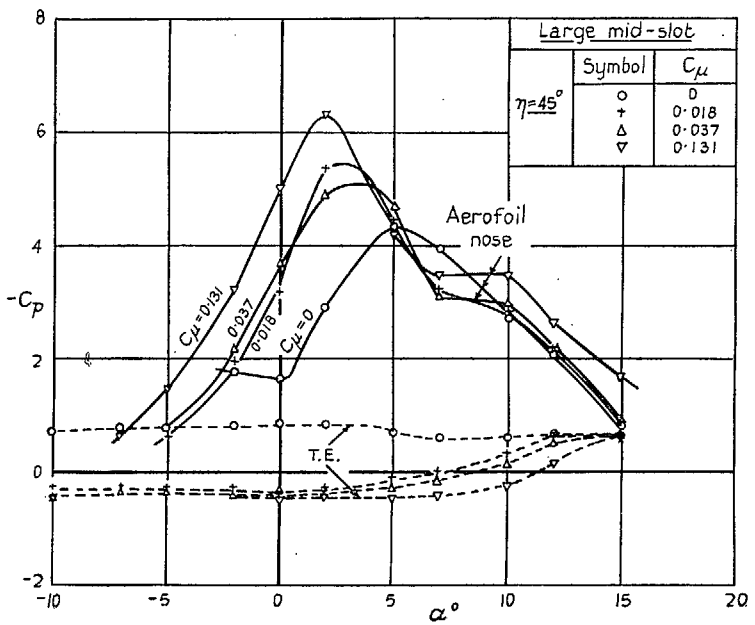

FIGS. 20a and 20b. Variation of peak suction measured on aerofoil nose and of trailing-edge pressure.

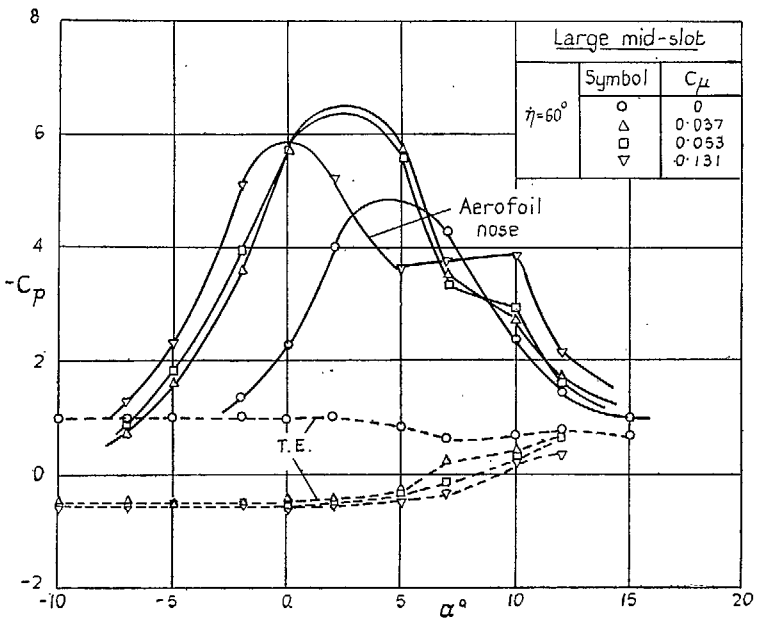

FIG. 20c. Variation of peak suction measured on aerofoil nose and of trailing-edge pressure.

32

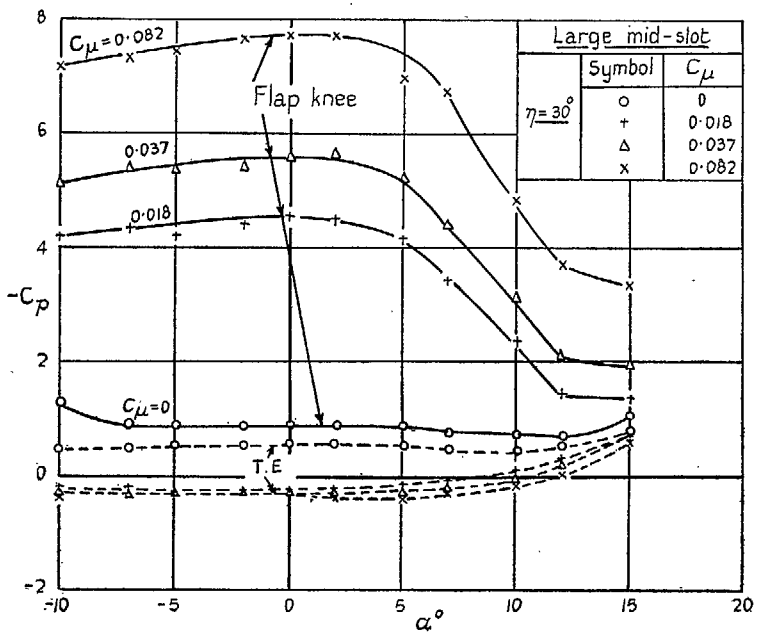

FIG. 21a. Variation of peak suction measured on flap knee and of trailing-edge pressure.

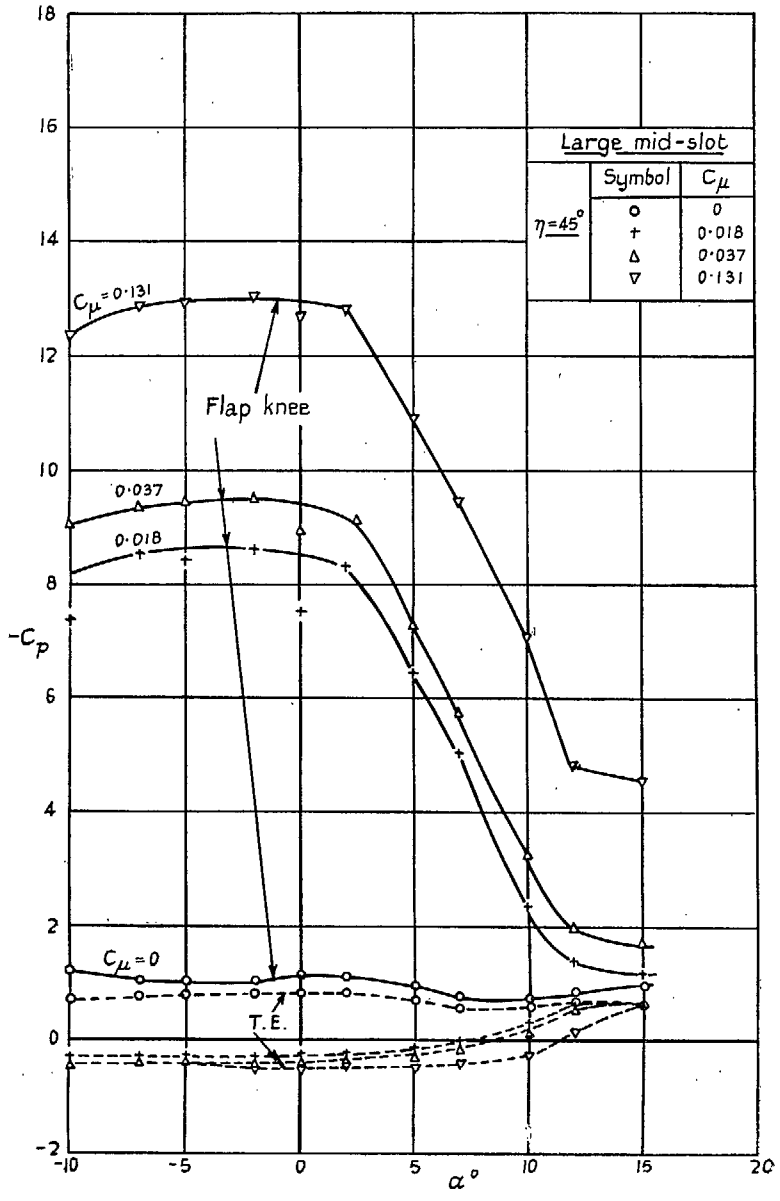

FIG. 21b. Variation of peak suction measured on flap knee and of trailing-edge pressure.

(72582) Wt. 52 K7 6/58 Hw.

PRINTED IN GREAT BRITAIN

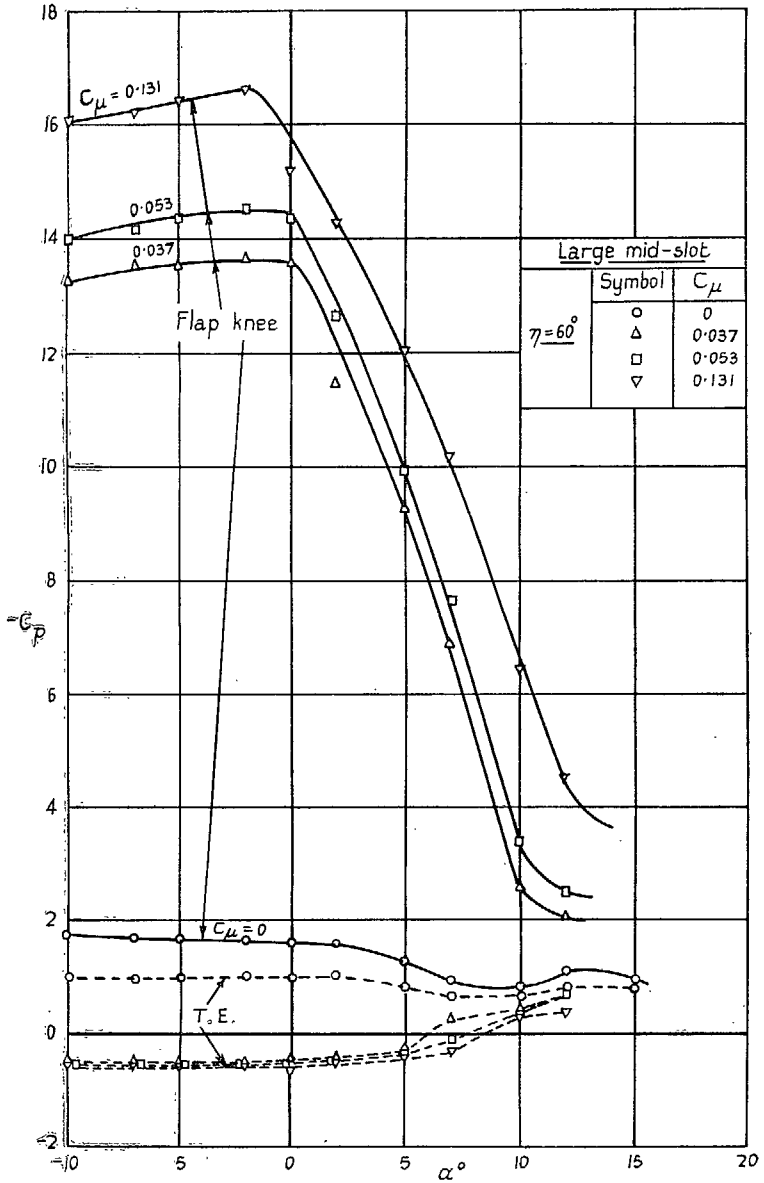

FIG. 21c. Variation of peak suction measured on flap knee and of trailing-edge pressure.

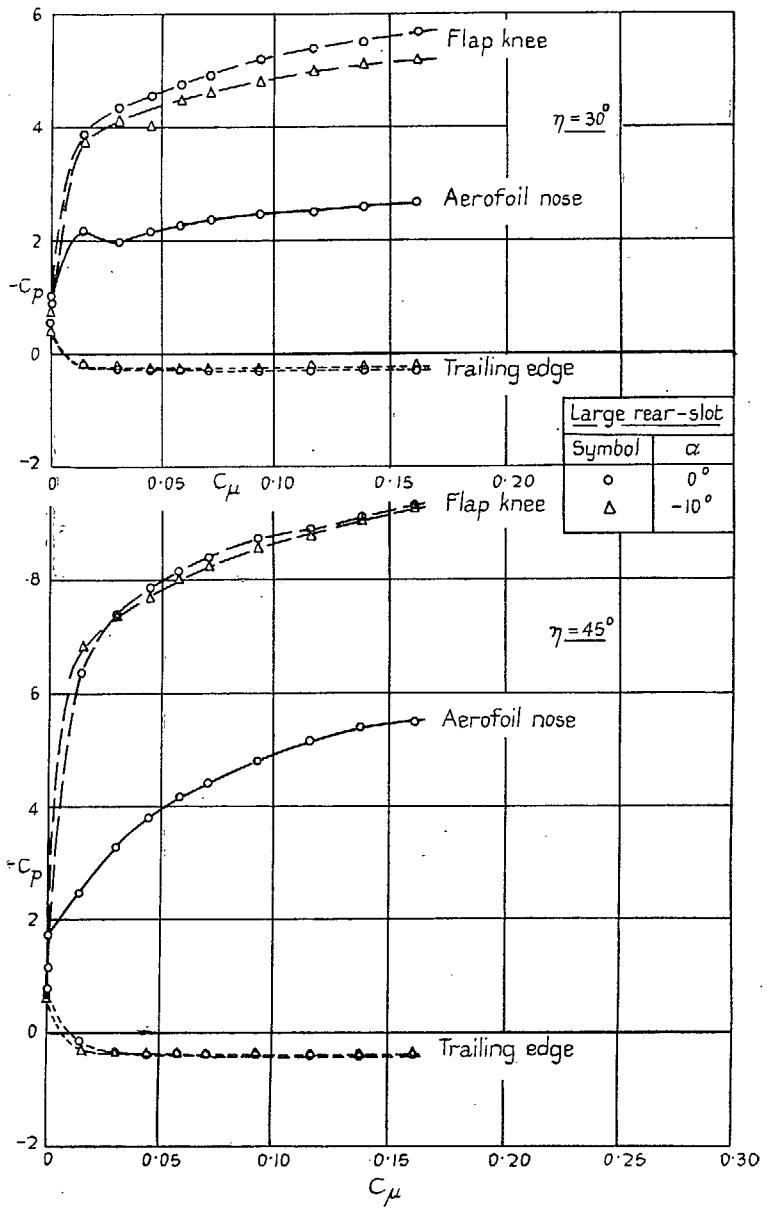

FIG. 22. Variation of peak suctions and trailing-edge pressure with C_μ at constant incidence.

Publications of the Aeronautical Research Council

ANNUAL TECHNICAL REPORTS OF THE AERONAUTICAL RESEARCH COUNCIL (BOUND VOLUMES)

1939 Vol. I. Aerodynamics General, Performance, Airscrews, Engines. 50*s.* (52*s.*).
Vol. II. Stability and Control, Flutter and Vibration, Instruments, Structures, Seaplanes, etc. 63*s.* (65*s.*)

1940 Aero and Hydrodynamics, Aerofoils, Airscrews, Engines, Flutter, Icing, Stability and Control, Structures, and a miscellaneous section. 50*s.* (52*s.*)

1941 Aero and Hydrodynamics, Aerofoils, Airscrews, Engines, Flutter, Stability and Control, Structures. 63*s.* (65*s.*)

1942 Vol. I. Aero and Hydrodynamics, Aerofoils, Airscrews, Engines. 75*s.* (77*s.*)
Vol. II. Noise, Parachutes, Stability and Control, Structures, Vibration, Wind Tunnels. 47*s.* 6*d.* (49*s.* 6*d.*)

1943 Vol. I. Aerodynamics, Aerofoils, Airscrews. 80*s.* (82*s.*)
Vol. II. Engines, Flutter, Materials, Parachutes, Performance, Stability and Control, Structures. 90*s.* (92*s.* 9*d.*)

1944 Vol. I. Aero and Hydrodynamics, Aerofoils, Aircraft, Airscrews, Controls. 84*s.* (86*s.* 6*d.*)
Vol. II. Flutter and Vibration, Materials, Miscellaneous, Navigation, Parachutes, Performance, Plates and Panels, Stability, Structures, Test Equipment, Wind Tunnels. 84*s.* (86*s.* 6*d.*)

1945 Vol. I. Aero and Hydrodynamics, Aerofoils. 130*s.* (132*s.* 9*d.*)
Vol. II. Aircraft, Airscrews, Controls. 130*s.* (132*s.* 9*d.*)
Vol. III. Flutter and Vibration, Instruments, Miscellaneous, Parachutes, Plates and Panels, Propulsion. 130*s.* (132*s.* 6*d.*)
Vol. IV. Stability, Structures, Wind Tunnels, Wind Tunnel Technique. 130*s.* (132*s.* 6*d.*)

Annual Reports of the Aeronautical Research Council—

1937 2*s.* (2*s.* 2*d.*) 1938 1*s.* 6*d.* (1*s.* 8*d.*) 1939–48 3*s.* (3*s.* 5*d.*)

Index to all Reports and Memoranda published in the Annual Technical Reports, and separately—

April, 1950 - - - - R. & M. 2600 2*s.* 6*d.* (2*s.* 10*d.*)

Author Index to all Reports and Memoranda of the Aeronautical Research Council—

1909—January, 1954 R. & M. No. 2570 15*s.* (15*s.* 8*d.*)

Indexes to the Technical Reports of the Aeronautical Research Council—

December 1, 1936—June 30, 1939	R. & M. No. 1850	1*s.* 3*d.* (1*s.* 5*d.*)
July 1, 1939—June 30, 1945	R. & M. No. 1950	1*s.* (1*s.* 2*d.*)
July 1, 1945—June 30, 1946	R. & M. No. 2050	1*s.* (1*s.* 2*d.*)
July 1, 1946—December 31, 1946	R. & M. No. 2150	1*s.* 3*d.* (1*s.* 5*d.*)
January 1, 1947—June 30, 1947	R. & M. No. 2250	1*s.* 3*d.* (1*s.* 5*d.*)

Published Reports and Memoranda of the Aeronautical Research Council—

Between Nos. 2251–2349	R. & M. No. 2350	1*s.* 9*d.* (1*s.* 11*d.*)
Between Nos. 2351–2449	R. & M. No. 2450	2*s.* (2*s.* 2*d.*)
Between Nos. 2451–2549	R. & M. No. 2550	2*s.* 6*d.* (2*s.* 10*d.*)
Between Nos. 2551–2649	R. & M. No. 2650	2*s.* 6*d.* (2*s.* 10*d.*)
Between Nos. 2651–2749	R. & M. No. 2750	2*s.* 6*d.* (2*s.* 10*d.*)

Prices in brackets include postage

HER MAJESTY'S STATIONERY OFFICE

York House, Kingsway, London W.C.2; 423 Oxford Street, London W.1; 13a Castle Street, Edinburgh 2; 39 King Street, Manchester 2; 2 Edmund Street, Birmingham 3; 109 St. Mary Street, Cardiff; Tower Lane, Bristol 1; 80 Chichester Street, Belfast, *or through any bookseller.*

S.O. Code No. 23-3087